CHEMICAL PROPULSION RESEARCH AT MSFC

6

January 26, 1967

By

Keith B. Chandler
Peter G. Haas
Robert R. Head
James R. Thompson, Jr.
Ralph G. Weitenbeck

CONTENTS...

IMPROVED FLUID CONNECTORS

by Peter G. Haas

LIST OF TABLES

LIST OF ILLUSTRATIONS

MAIN SEAL TECHNOLOGY FOR VENT VALVES

by Ralph G. Weitenbeck

CONTENTS (Continued)...

LIST OF TABLES

LIST OF ILLUSTRATIONS

FLUID MECHANICS

by Robert R. Head

LIST OF ILLUSTRATIONS

CONTENTS (Continued)...

LARGE ENGINE TECHNOLOGY

by Keith B. Chandler

LIST OF TABLES

LIST OF ILLUSTRATIONS

CONTENTS (Continued)...

J-2 EXPERIMENTAL ENGINEERING PROGRAM (J-2X)

by James R. Thompson, Jr.

LIST OF ILLUSTRATIONS

CONTENTS (Concluded)...

IMPROVED FLUID CONNECTORS

By

Peter G. Haas

SUMMARY

The requirement for reduced leakage and mass in space vehicles, and improved reliability and handling of fluid connectors called for advances in current technology. A major portion of Contract NAS8-11523, the feasibility study of a new semi-permanent connector, has demonstrated a successful fluid connector design concept which could lead to replacing most of the separable connectors in future space vehicles with the semi-permanent connectors. The design features, tooling concept, and development steps are discussed, and test data are given in this report. While the last task of the technology contract (combined environmental tests) is being concluded, a new contract (NAS8-20572) proceeds to develop all sizes of the new connector design and perform a formal qualification test.

INTRODUCTION

Statistical review of Launch vehicle fluid connections indicates a marked trend toward separable connectors (flanged or threaded joints) instead of the usual brazed or welded permanent connections (Fig. 1). This trend is caused by the many advantages of separable connection such as ready access to subassemblies for test or checkout purposes, easy quality control, consistent performance, and high experience level.

PERMANENT	20 %
SEPARABLE	80 %
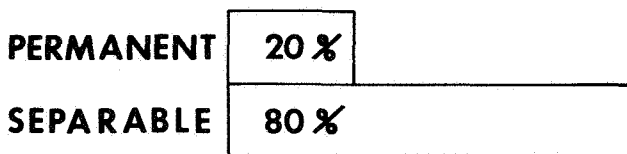
FIGURE 1. PRESENT FLUID CONNECTORS

Since there are more than 9000 joints in some vehicles, the extent of the 4 to 1 ratio in Figure 1 should be examined, especially for an operational vehicle.

A closer look at statistics on the sizes of the separable connectors reveals that the majority of the connectors are in the "tube range," below 0.038 m (1 1/2 in.) outside diameter (Fig. 2). One-sixth of the connectors are constructed from aluminum alloys, the rest are stainless steel.
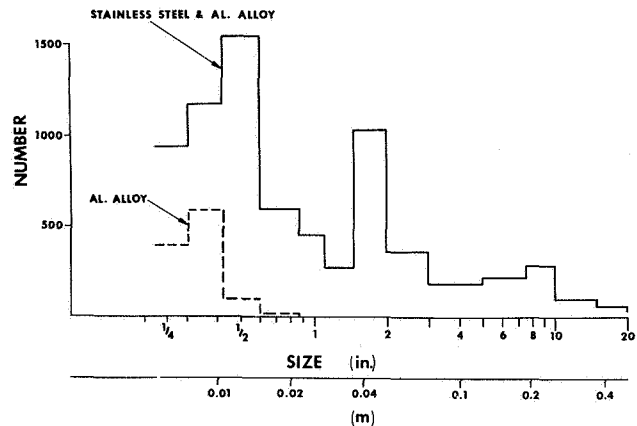
FIGURE 2. PRESENT FLUID CONNECTORS

Semi-permanent Connectors. Most of these tube connectors do not need to be reassembled for an unlimited number of times, yet their operation does exceed the restrictions of a permanent assembly. Combining the features of a permanent joint -- extremely low leakage, minimum relaxation of sealing members -- with the option of a limited number of reassemblies -- three to four times before major rework--resulted in establishing the semi-permanent connector concept (Fig. 3).

The preferred concept of a semi-permanent connector is certainly mechanical because (1) inherently easier quality control enhances reliability, (2) clean reassembly prevents contamination of the system, and (3) minimum mass of the complete system is assured since the tube maintains its strength at the connector interface.
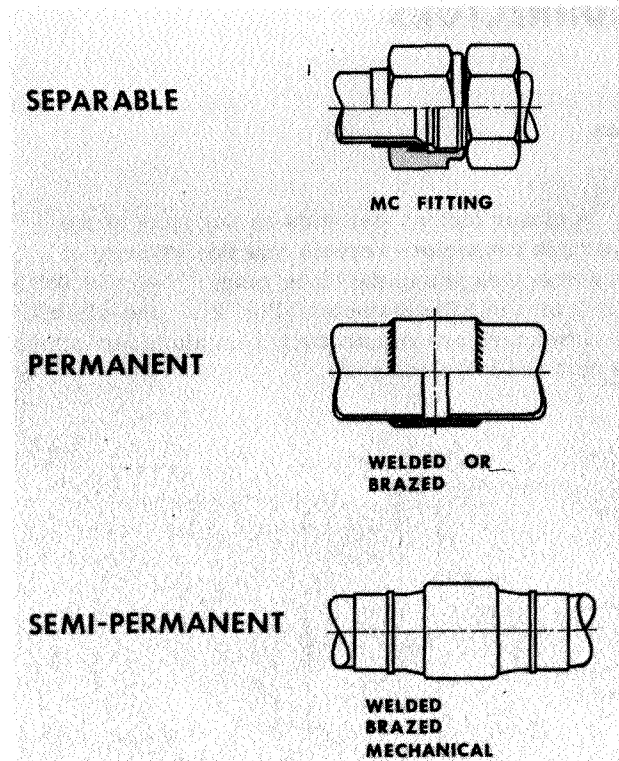
FIGURE 3. TUBE CONNECTIONS

FEASIBILITY STUDY ON THE X-CONNECTOR

A connector (the X-connector) is being developed by the Parker Aircraft Company* to meet the required characteristics (Fig. 4). In terms of the design, the operational requirements are (1) The material shall be Stainless Steel, (2) The primary size range is 0.0063 through 0.0317 m (1/4 through 1 1/4 in.), (3) The temperature range is 19° K (-425° F) to 645° K (700° F), (4) The operating pressure is 3.1×10^7 N/m² (4500 psi) for high pressure systems, and 0.69×10^7 N/m² (1000 psi) for low pressure systems, (5) Field assembly and reassembly of the connectors is practical, and (6) Leakage is below 10^{-12} m³/s (10^{-6} cc/s) of Helium at standard conditions. Futhermore, essential design objectives must be verified such as (1) consistent assembly performance, (2) positive quality assurance, (3) minimum connector mass, (4) no restriction on tubing material condition, (5) possible standardization of parts for any configuration, (6) concept adaptable to duct sizes [0.038 m (1 1/2 in.) and up], (7) practical production and easy handling, and (8) low cost.

The present effort is to develop the connector for the 0.0127 m (1/2 in.) tube size only, to demonstrate the feasibility of the concept. The

TUBE MATERIAL: SS 304 L, $\frac{1}{8}$ HARD
(MSFC-SPEC 131)
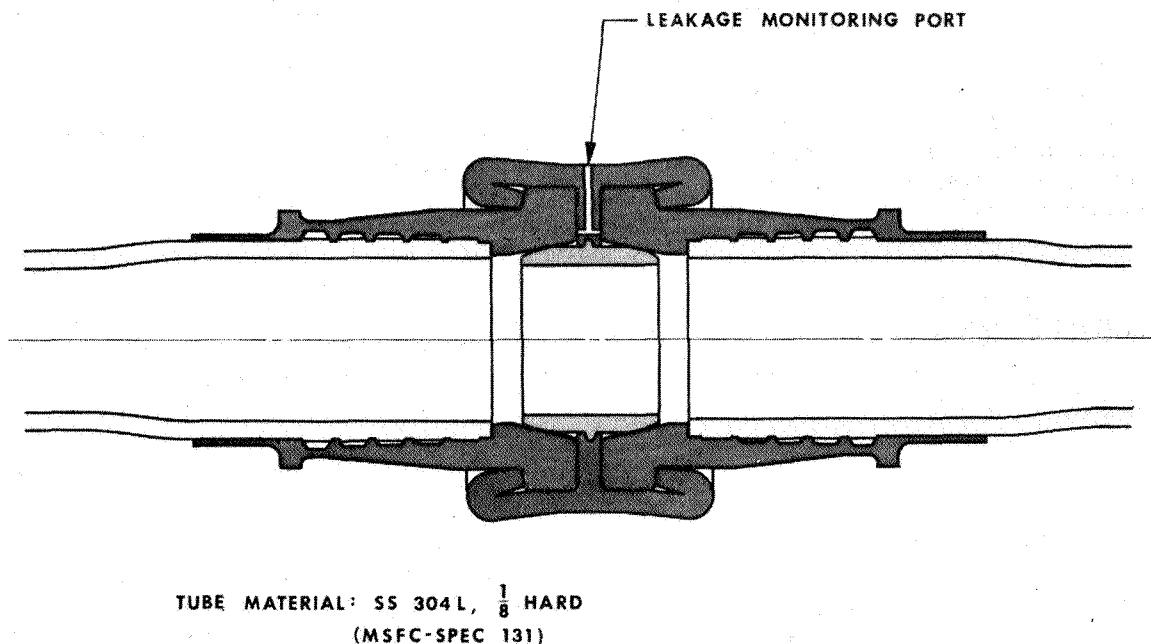
FIGURE 4. X-CONNECTOR

* Subcontractor in Contract NAS8-11523 with General Electric (Table I) and contractor in NAS8-20572.

TABLE I. CONTRACT NAS8-11523

Zero-Leakage Design of Tube and Duct

Connectors for Deep Space Travel

    General Electric Co.

        Begin: June 29, 1963
        End: April 1, 1967 (Projected)

Parker Aircraft: Subcontractor for Feasibility
            Study on the X-Connector

Subcontract:

Phase I: Configuration
      Seal Concept
      Structural Members
      Tooling
      Performance Test and Evaluation
      Design Optimization

Phase II: Feasibility Demonstration
      Sample Production
      Verification Tests

          Proof & Burst Pressure
          Leakage
          Tension Load

      Combined Environmental Tests

      Leakage
      Temperature Extremes
      Vibration

FIGURE 5. X-CONNECTOR

seats the tube in the sleeve and expands the sleeve a predetermined amount. Springback of the sleeve exerts adequate residual forces. By embedding the contact rings into the tube surface, the sleeve is keyed to the tube and gives local, heavy deformation to penetrate surface imperfections. Optional gold plating of the internal sleeve surface eliminates existing tubing irregularities.

By stretching the sleeve-tube assembly beyond yield stress, the effect of their radial tolerances is nullified for swaging results.

The second shop operation is a collar-seal attachment process. This preassembly -- swaging of the seal to the collar -- is part of the production process of the components. In the original connector concept, collar and seal were one piece; however, for ease of fabrication a separate machining operation and preassembly was chosen. The permanent subassembly of both parts prevents installation of the connector without a seal and properly locates the seal at assembly.

Connector Assembly. With subassemblies made, the final in-place installation and collar connection is completed by another swaging operation (Fig. 7). The collar swaging tool, powered by hydraulic pressure, consists of the scissors assembly power pack and a splittable wedge assembly (detail A).

The sleeve flanges are engaged in the collar, and the swage tool is closed around the unformed

configuration of the X-connector has been set and includes the parts in Figure 5. The material for all connector parts is Nickelbase alloy 718 because of its high strength and excellent performance at extreme environments, and for good formability.

A locating ledge on the sleeve assures proper positioning of the tube. To transfer shear loads, the contacting rings, or lands, provide high-stress contacts with the mating tube. Also, the lands provide redundant seals. The reduced section in the skirt or fantail minimizes stress concentration in the transition region between connector and full tube, and can dampen during vibration. The sealing surface on the conical part of the sleeve is recessed and thus safe from damage. The collar links the two connector halves, and consists of two lips and stops for the sleeves. The seal engages the conical sealing surfaces of the sleeve with a high preload. Gold plating of the seal prevents galling at installation and fills any surface irregularities.

Two shop operations are needed to preassemble the connector. The first is swaging the sleeve to the tube end. The radial expansion tool (Fig. 6)

FIGURE 6. TUBE-SLEEVE SWAGING

DETAIL **A**
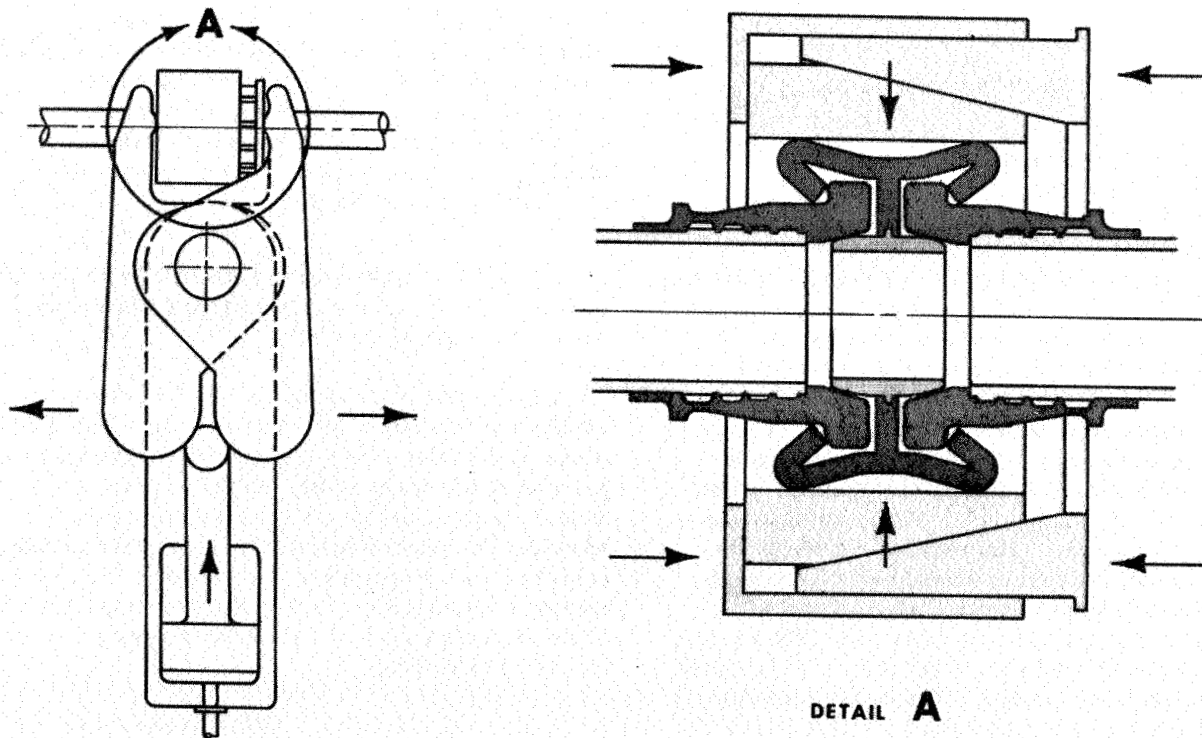
FIGURE 7. COLLAR SWAGING

connector. Closing the tool assures proper engage-
ment and alignment of the parts for adequate collar
forming. The tool is then tightened axially to keep
the parts in close engagement. Next, hydraulic
pressure is applied. The power causes a ring of
radially-moving wedges to form the x-shaped collar
into a cylinder. During this operation, the collar lips
move in radially to engage the sleeve flanges and
finally to drive the sleeves into the solid stop of the
collar, closing the high spring rate circuit of forces.

The toggle action of the collar drives the seals into their seats with a yielding action. This eliminates the effects of dimensional tolerances between seal and sleeve seat, and maintains ample seating stress for leaktight operation. The gold plate on the sealing surface shears into the asperities of the mating surface as a caulking compound.

The seating stresses at the edges of the collar top are high enough to make a secondary seal at the flange. Any leak from the primary seal area is collected at the monitoring port (Fig. 4).

Connector Separation. Separation and reassembly, vital to the semi-permanent connector concept, is achieved readily: to separate the connector, the collar lips are simply cut off to release the sleeve shoulders. Another mode is unswaging the collar.

A tool package -- similar to the wedge assembly of Figure 7 but with an inverse mechanism -- inserted in the swage power pack provides the means for unswaging and separation. After separation and disposal of the collar and seal, the tube ends are ready for reassembly with a new collar.

Significant features of the design concept of the mechanical, semi-permanent X-connector are that (1) The seal is not a main structural member. This basic design principle is demonstrated by the closed load loop consisting of the sleeve flange, collar stop, collar lips and sleeve shoulder. Large variations of forces on the coupling cause no motion of the flanges relative to the stops, and therefore do not endanger seal integrity, (2) For a leaktight seal, local stress of one seal member should be well above yield strength. The seal spring makes and sustains a high preload to yield the gold plate on the seal interface, (3) The mechanical, plastic deformation of mating connector parts (used extensively) has several advantages: yielding into place avoids critical tolerances and thus lowers production costs; better reproducibility of assembly operation requires fewer dimensional checks; permanent location of mating parts prevents disengagement and leakage; and work hardening gives greater effective strength of materials, (4) Optimum transfer of loads from the connector to the free tube by the reduced cross-section of the fantail area, and (5) Effective leakage monitoring of all four possible leak-paths: seal leakage monitoring at the central collar location, and tapping the sleeve between two lands for checkout of tube-sleeve swage leakage.

CONNECTOR DEVELOPMENT STATUS

Development of a 0.0127 m (1/2 in.) tube size connector started with three basic design-element investigations: swaged connection of tube and sleeve, collar forming, and seal performance. After a series of iterations -- redesign, test and evaluation of likely candidates -- integration of the most effective basic components into a connector was achieved.

The iterative development effort on the element level included:

1. Tube-sleeve swage: variation of tube wall thickness and material strength, variation of the number of sleeve lands, variation of sleeve yielding.

2. Collar forming: variation of material, forming tool study, collar cross-section as a parameter, forming motion study.

3. Seal performance: variation of materials, gold plating study, seal penetration study.

Testing of final configurations demonstrated adequate performance under tensile load, in vibratory fatigue with and without heat load, and under impulse and burst pressures. Mass spectrometer leak measuring was done during or after tests to verify that leakage was below 10^{-6} scc/s of Helium.

Subsequently, complete 0.0127 m (1/2 in.) connectors were designed, fabricated, and tested. In Figure 8 leakage test results are listed for eight connectors. The tests were made to assess quality and reliable fabrication of tube-sleeve swages of connector assemblies by measuring leakage across singular lands. Indicated leak-rates occurred at proof pressure level of 6.21×10^7 N/m^2 (9000 psi); there was no excessive leakage at the rated pressure of 3.10×10^7 N/m^2 (4500 psi). "Leakage of full connector" denotes leakage monitoring across all lands (no monitoring holes) using long-duration-pressure application to avoid the effect of leakage-flow delay caused by the series of voids between the

sleeve lands. The vibration tests were performed for 10^6 cycles at stress levels up to 2.42×10^8 N/m^2 (35 ksi). Stress levels were defined as the maximum fiber stress on the tube adjacent to the connector.

LEAKAGE MEASUREMENT: He MASS SPECTROMETER
SENSITIVITY 2×10^{-14} m^3/s $(2 \times 10^{-8}$ scc/s)

TEST PRESSURE: 6.21×10^7 N/m^2 (9000 psi) (PROOF PRESSURE)

LEAKAGE OF SINGULAR LANDS (①) TO (⑤))
12 ASSEMBLIES: 3 EVENTS BEFORE } VIBRATION
0 EVENTS AFTER

LEAKAGE OF FULL CONNECTOR (⑥),(⑦))
4 ASSEMBLIES: NONE
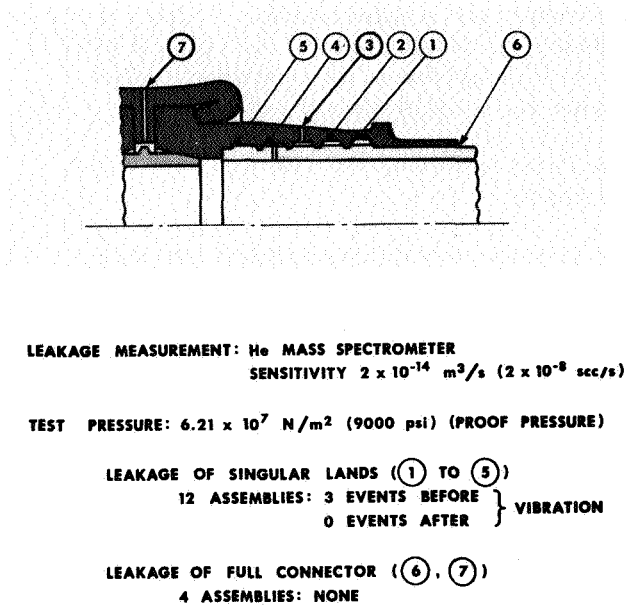
FIGURE 8. LEAKAGE TESTS

Test results of connector assemblies under impulse, tensile, and burst tests are indicated in Figure 9.

IMPULSE TESTS

    Peak Pressure = I.5 Operating Pressure
    10,000 Cycles
    No Leakage
    No Damage

TENSILE TESTS

    Tensile Load = 4 x End Load Caused by Operating Pressure.
    No Connector Failure

BURST TESTS

    Burst Pressure = 4 x Operating Pressure
    No Connector Failure

FIGURE 9. CONNECTOR ASSEMBLY
TEST RESULTS

Comparative fatigue test results are shown in Figure 10. Reduction of fatigue strength caused by the stress discontinuity induced by the connector appears as the slope change in the logarithmic fatigue chart. Unfortunately, no comparative values from other connector types are yet available.
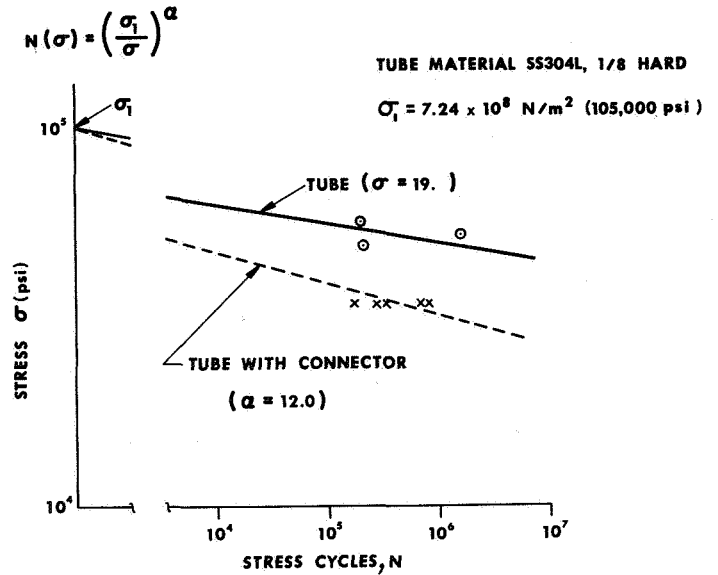
FIGURE 10. FATIGUE TESTS

After completion of the test series the final attempt at feasibility demonstration of the X-connector concept is underway in a series of combined environmental tests. The test program with 26 connector samples includes (1) leakage and proof pressure for hardware checkout, (2) low temperature (LN$_2$) at operating pressure, with mass spectrometer leakage monitoring, (3) high temperature [645° K (700° F)] at operating pressure, with leakage measurement, (4) high temperature at operating pressure, under vibration, with leakage measurement, and (5) long-duration measurement of leakage of several connectors (sleeves without leakage monitoring capability). All other assemblies have monitoring holes tapping the first sleeve void (between land 3 and 4 of Fig. 8).

FUTURE EFFORT

Presently, the X-connector design and development in Contract NAS8-20572 are attempted for the standard tube sizes 0.0063, 0.0095, 0.0127, 0.0191, 0.0254, 0.0317 m (1/4, 3/8, 1/2, 3/4, 1, 1 1/4 in.) and associated tooling (Table II). This effort includes two operating pressure levels: the previously

TABLE II. CONTRACT NAS8-20572

Development and Qualification of Improved
Fluid Connectors
Parker Aircraft Co
Begin: June 29, 66
End: June 29, 68 (Proj.)

Phase I: Design and Evaluation
            -Develop all Standard Tube Sizes
            -Develop Tooling

Phase II: Production
            -Qualification Samples
            -Tooling

Phase III: Qualification

Phase IV: Documentation

defined 3.1×10^7 N/m^2 (4500 psi), and 0.69×10^7 N/m^2 (1000 psi) for low-pressure applications. The definition of low-pressure tubing will result in extensive system mass reduction, particularly in the larger tube sizes.

The development program will be continued in a production phase to form connector samples and tooling, and a test phase for flight qualification of the X-connector. Immediate application of the connectors on flight vehicles is then planned.

MAIN SEAL TECHNOLOGY FOR VENT VALVES

By

Ralph G. Weitenbeck

SUMMARY

A program was implemented to improve the effectiveness of large-diameter vent valves for use in the LOX, fuel, and helium systems of space vehicles. At the time the development contract was signed, the norm for leakage of the valve under consideration was 67 scc/s. Areas of work on the vent valve included the bellows, actuators, shaft and main seals. Of main importance was the work done on the main seal. Leakage test results were in the order of 1.0 scc/s at 505° K (450° F), 1.0 scc/s at 295° K (70° F), and 11.0 scc/s at 77.5° K (-320° F).

INTRODUCTION

The main seal evaluation phase of the program consisted of the study, testing, and development of a valve seal of a flapper and seat arrangement. The operational requirements were as follows: (1) size, 25.4 cm (10 in.) internal diameter, (2) pressure, 0 to 344 000 N/m² (0 to 50 psig), (3) temperature, 77.5° K to 505° K (-320° F to +450° F), (4) leakage, 13.7 scc/s nitrogen, and (5) life, 2000 cycles.

DESIGN APPROACH

The initial design approach was to use a moving member (flexible flapper) to seat against a thin land on a fixed seat. For rigidity of the flapper when working close to the seat, a stiff backup member supported the flapper as it rose off the seat. Seating load was maintained by the pressure force acting over the area of the flapper. Relatively little change in design concept occurred during development.

Choice of flapper material was based on (1) high tensile strength at elevated temperatures, and (2) good impact strength at cryogenic temperatures. The materials considered and their significant mechanical properties are in Table I. Of these materials, Inconel 718 had the highest tensile strength at a high temperature of 589° K (+600° F) and also demonstrated acceptable impact strength at a cryogenic temperature of 77.5° K (-320° F). This material gives the lightest possible flapper.

TABLE I. SIGNIFICANT MECHANICAL PROPERTIES OF MATERIALS CONSIDERED FOR 25.4 cm (10 IN.) FLAPPER

Mechanical Properties in N/m²×10⁵(psi×10³)	A-286	Inconel-X	Inconel-718
Tensile Strength at Room Temperature	9.64(140)	13.4(195)	13.8 (200)
Tensile Strength at 589° K (600° F)	8.26(120)	9.64(140)	12.7 (185)
Yield Strength at Room Temperature	6.20(90)	9.64(140)	11.7 (170)
Yield Strength at 589° K (+600° F)	5.16(75)	8.26(120)	10.7 (155)
Impact Strength Charpy V-Notch at 77.5° K (-320° F)	3.44-4.13 (50 - 60)	2.06-2.76 (30 - 40)	1.24 (18)

In the development work five (5) flapper and seat configurations were designed and tested, each new configuration evolving from test information of the preceding configurations. The nominal seal, configuration No. 1, came from these considerations: (1) The flapper must be flexible enough to conform to waviness in the seat caused by thermal and pressure stresses, (2) Since the flapper is flexible, a rigid backup support must be incorporated to prevent flutter and buzz, and (3) The seat and flapper materials must be of sufficient hardness to prevent galling and wear.

The most significant problem inherent in configurations 1 through 4 was an high-impact unit loading caused by the fast closure speed. The closure time of 40 msec was increased to 175 msec before testing configuration No. 5.

Also, after further study of the seal configuration, a configuration of Inconel 718 flapper material and seat material of A-286 was tested again. The reasons for this change were (1) The softer material in a flapper and seat combination will be deformed during use, (2) The narrower member in a seat and flapper combination should be constructed of the softer material. This will, in effect, deform the entire surface of the narrow member and allow the wide member (flapper) to shift slightly from cycle to cycle without impairing sealing quality, (3) A-286 is a relatively softer material than Inconel 718 and so was the logical choice for the narrower member (the seat), and (4) The stronger (harder) material should be used for the flapper to allow building a lighter weight part.

Configuration No. 5 (Fig. 1 and 2) was subjected to 7900 endurance cycles. The leakage at 344 000 N/m² (50 psig) at room temperature did not exceed 1.4 scc/s nitrogen. After the 7900 endurance cycles the seat and flapper were disassembled, inspected, and reinstalled in the test fixture.

FIGURE 2. FLAPPER AND SEAT ARRANGEMENT DETAIL "A"

Leakage tests at 505° K (+450° F), room ambient and 77.5° K (-320° F) were performed with N_2 and He gas. The results of this test are in Table II. This highly successful test verified the acceptability of the final design.

TABLE II. LEAKAGE RESULTS AFTER 7900 CYCLES

Temp °K	Pressure N/m² × 10⁵ (psig)	Medium	Leakage scc/s
505 (450° F)	3.44 (50)	GN_2	<1.0
505 (450° F)	1.72 (25)	GN_2	<1.0
505 (450° F)	3.44 (50)	He	<1.0
505 (450° F)	1.72 (25)	He	<1.0
Room	3.44 (50)	GN_2	1.0
Room	1.72 (25)	GN_2	1.0
Room	3.44 (50)	He	1.3
Room	1.72 (25)	He	1.2
77.5 (-320° F)	3.44 (50)	GN_2	10.9
77.5 (-320° F)	1.72 (25)	GN_2	6.3*
77.5 (-320° F)	3.44 (50)	He	26.0
77.5 -320° F	1.72 (25)	He	17.5**

* Present Norm = 67 scc/s
** Present Norm = 133 scc/s

FIGURE 1. FLAPPER AND SEAT ARRANGEMENT

10

The test fixture (Fig. 3) consisted of a simple pneumatic actuator operated at 5.16×10^6 N/m^2 (750 psi), 2 bar linkage arrangements, and the seal configuration.

CONCLUSION

Evaluation of the results of the development tests verified the success of the program and confirmed that it was possible to produce a metal-to-metal seal to reliably meet low-leakage requirements. The results of this development were further confirmed by successful completion of a 25.4 cm (10 in.) LOX Vent and Relief Valve Program in which this seal was used. Overall excellent valve performance was demonstrated in meeting the 13.7 scc/s leakage requirement through a temperature band of 505°K to 77.5°K (+450°F to -320°F) (Figs. 4 and 5).

FIGURE 3. ASSEMBLY OF TEST FIXTURE AND SEAT CONFIGURATION

FIGURE 4. 25.4 cm (10 in.) LOX VENT AND RELIEF VALVE

VALVE CLOSED   VALVE OPEN

FIGURE 5. 25.4 cm (10 in.) LOX VENT AND RELIEF VALVE SCHEMATIC

FLUID MECHANICS

By

Robert R. Head

SUMMARY

Three areas of inhouse research in fluid mechanics are discussed: bubble dynamics, two-phase flow and flow measurement by laser Doppler shift.
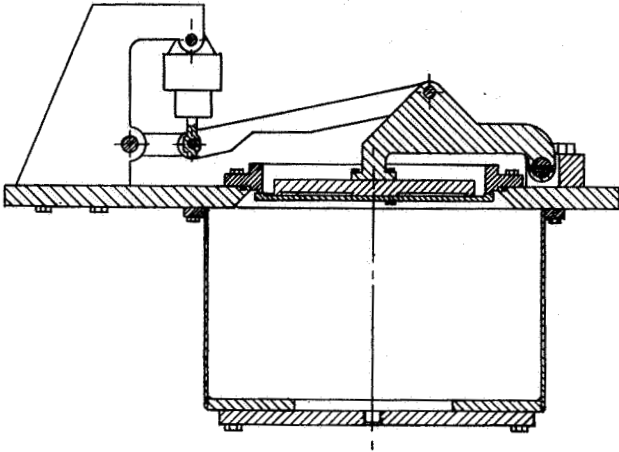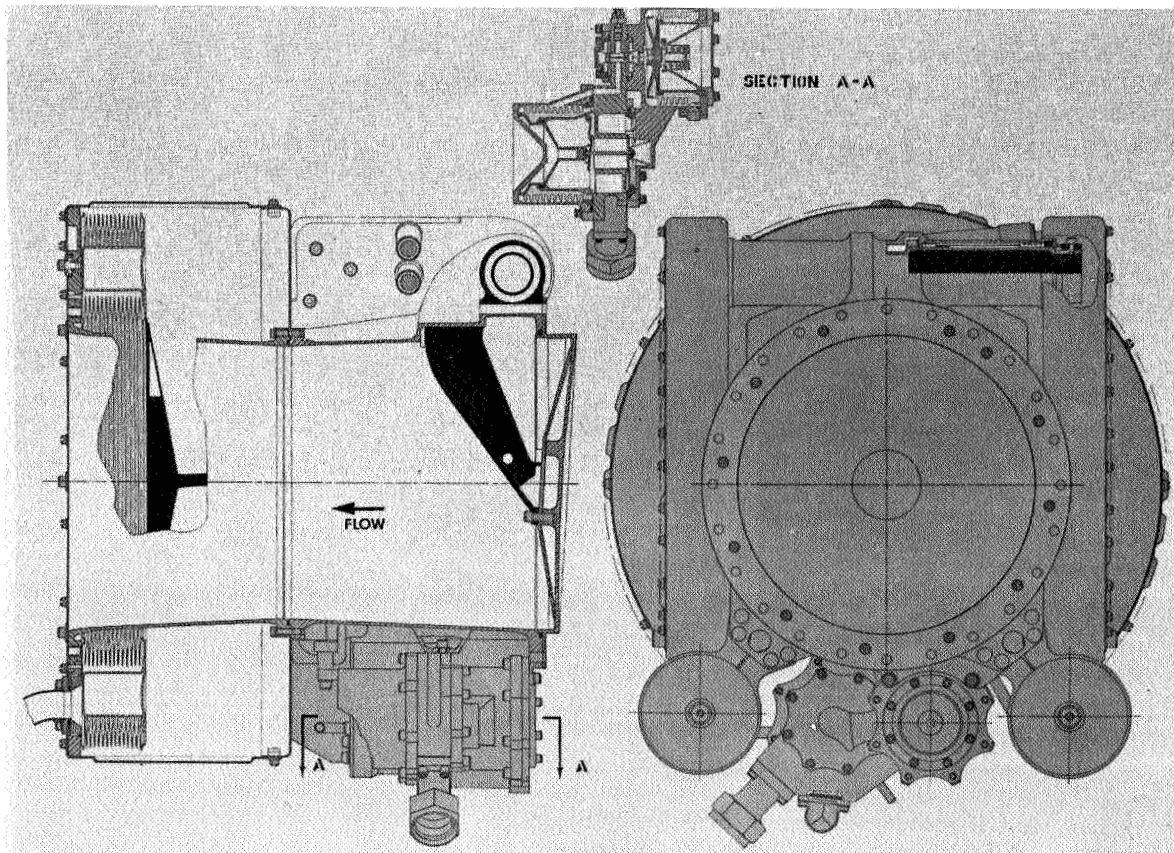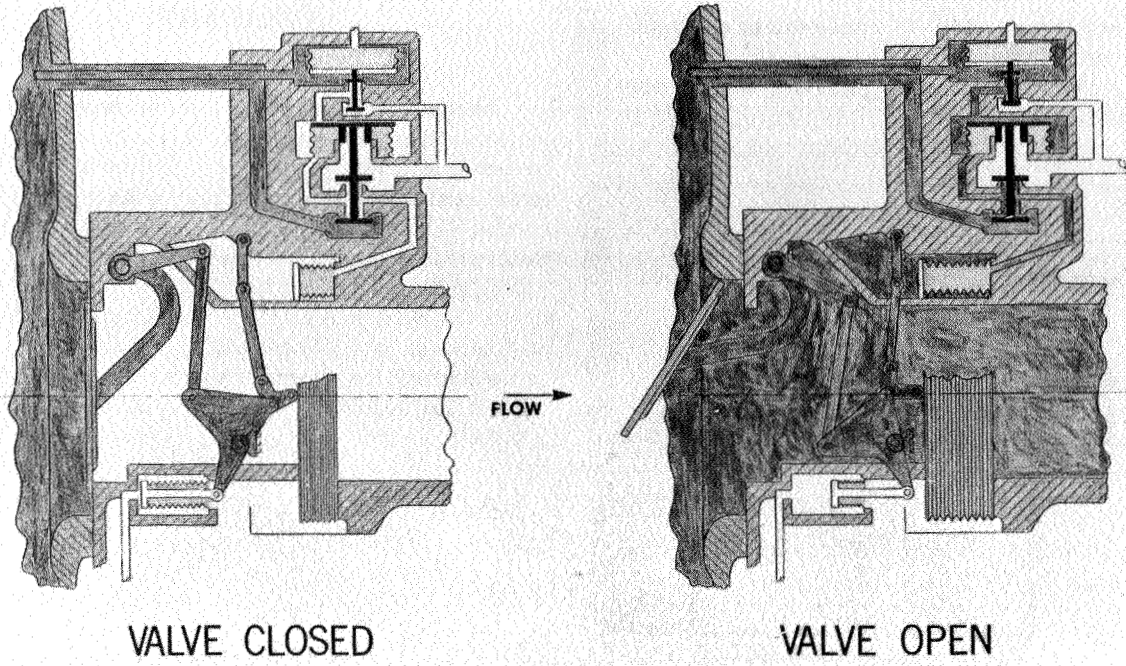
Bubble Dynamics. Terminal velocities were determined for an inert gas injected as a single bubble into an LN_2 column. A dimensionless parameter was found, which together with the classical dimensionless parameters permits experimental simulation of low g (gravity) effects at one g.

Liquid columns of water and methanol were longitudinally vibrated within the frequency range experienced on launch vehicles, and the bubbles and bubble clusters were studied. Mathematical expressions were obtained that define the condition for inception.

Two-Phase Flow. Two-phase flow in cryogenic systems was experimentally investigated and compared with the theoretical models for frozen equilibrium and shifting equilibrium. Analysis of two-phase flow as a single component was found by the frozen equilibrium model to be accurate for qualities above thirty-five percent.

Flow Measurement by Laser Doppler Shift. A laser velocimeter operating from the principle of the Doppler shift was used to investigate point velocities in a turbulent fluid flowing in a pipe. There was no protuberance of the flow stream. The velocity distribution was determined at each point and for each rate of bulk flow stream. The frequency response of the base instrument and electronics is sufficient to measure all frequencies of turbulence investigated.

The data were verified by comparing the mean velocity profile calculated from the probability distribution function with profiles determined by other methods of mean velocity measurement. The variance of the distribution function was verified by comparison with data on turbulent diffusion. The velocity distribution function as derived from statistical reasoning was found to properly describe the measured axial velocity components. The change in the variance of the velocity distribution function is derived and is compared with the measured variance.

DYNAMICS OF HELIUM BUBBLES IN LN_2

INTRODUCTION

The voids in liquids, called bubbles, consist of vapor from the parent liquid, dissolved or captured gases, inert gases in the liquid or combinations of these. Gas bubbling has been advantageously employed in our missiles and space vehicles. On the Jupiter vehicle, gaseous nitrogen was injected into the fuel line to prevent freezing in the line and stratification in the fuel tank. The same is employed in the first stage of the Saturn I and Saturn V vehicles. The principal objective is mass transfer. In the suction lines of the cryogenic propellants for most stages of the Saturn I and V vehicles, gaseous helium is injected for the primary purpose of cooling the propellants, although some mass transfer is present. In the case of cryogenic propellants the vapor pressure is relatively high and cooling occurs from the liquid flashing into the voids created by the helium bubbles.

Disadvantages from bubbles are those such as flow restrictions caused by cavitation, noise and vibration resulting from rapid bubble collapse and flashing caused from static pressure drop. Also there are bubbles produced by vibrating surfaces. In one case it was found that bubbles produced on a vibrating liquid level sensor caused erroneous readings.

In an attempt to have a better understanding of the phenomena and mechanics of bubbles, inhouse and contracted research studies have been initiated. In recent years extensive studies have been made relating to bubble motion, mechanism, and nucleations, both because of their technological implications and because it is a fascinating scientific problem encompassing many studies.

In nearly all papers on the motion of bubbles in liquids, the authors have recognized the following

factors as pertinent: bubble velocity, V, gravity, g, gravitational constant, g_c, liquid density, ρ_1, gas density, ρ_g, viscosity, μ, surface tension, σ, pressure, P, and bubble radius, R.

Although this list does not complete the set of quantities needed to specify the system, the effects of other factors are believed to be negligible.

It is possible to group these factors into five dimensionless parameters in terms of which the nine physical quantities can be described.

Reynolds Number, $\pi_{Re} = \dfrac{\overline{V}\rho R}{\mu} = \dfrac{\text{inertial force}}{\text{viscous force}}$, and relates dynamic similarity.

Froude Number, $\pi_{FR} = \dfrac{\overline{V}^2}{g\,R}$, $\dfrac{\text{inertial force}}{\text{gravitational force}}$, and relates to wave and surface behavior.

Weber Number, $\pi_{We} = \dfrac{\overline{V}^2\rho R}{g_c\,\sigma} = \dfrac{\text{inertial force}}{\text{surface tension}}$, and relates to bubble formation.

Drag Coefficient, $\pi_D = \dfrac{(\rho_1 - \rho_g)Rg}{\rho\,\overline{V}^2} = \dfrac{\text{gravitational force}}{\text{inertial force}}$, and relates to free settling velocity.

Bond Number, $\pi_{Bo} = \dfrac{(\rho_1 - \rho_g)R^2 g}{g_c\,\sigma} = \dfrac{\text{gravitational force}}{\text{surface tension}}$, and relates to breakup of bubble.

$G_1 = \dfrac{g\mu^4}{\rho\,\sigma^3} = \dfrac{N_{We}^3\,N_{FR}}{N_{Re}^4}$ and relates to pressure gradient.

Therefore, reasonable correlation is provided between bubbles rising in different fluids when plotted in terms of the above dimensionless parameters.

The first aspect of bubble dynamics studies involved high speed photographic observation of single bubbles and clusters of bubbles injected into a cryogenic liquid column.

EXPERIMENTATION

The experimental study covered gas bubble dynamics for terminal velocity, bubble collapse and natural bubble frequency. The experimental facility was designed to obtain the maximum information and still provide flexibility, to verify dimensionless parameters, and to study bubble collapse and bubble natural frequency for various gases in a cryogenic fluid.

One of the most difficult problems was to produce only a single bubble in a cryogen. Liquid nitrogen was used as the non-volatile liquid component in all cases. The gases injected were helium and nitrogen.

The diagram for gas flow, pressure control, and instrumentation is shown schematically in Figure 1.
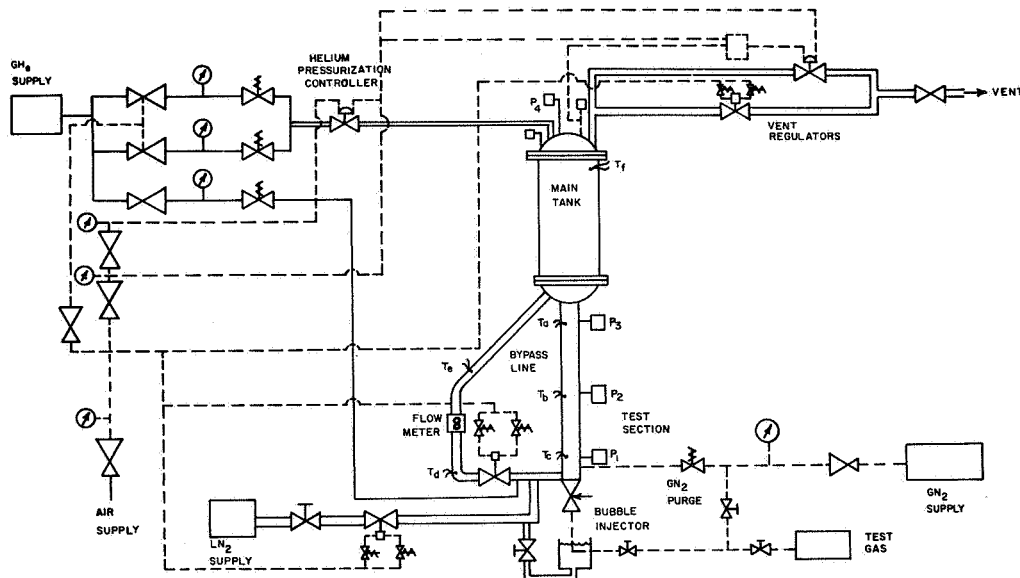

FIGURE 1. SCHEMATIC DIAGRAM FOR GAS FLOW, PRESSURE CONTROL AND INSTRUMENTATION

The test gas used in the experiment was passed from the cylinder equipped with pressure regulator through a chill bath of liquid nitrogen before entering the bubble injector. A needle valve with a micro- meter attachment was used to adjust the rate of gas for bubble injection.

The tank pressure can be adjusted between atmospheric pressure and 0.34×10^6 N/m^2 (50 psig) by injecting helium above the liquid in the tank. The rate of pressurization can be controlled. The vent regulator, which was situated on the top of the tank, was set for a maximum pressure of 0.34×10^6 N/m^2 (50 psig). The tank pressure was measured by Wiancko transducers, monitored by strip chart recorder and recorded on an oscillograph. Pressure is read to $\pm 0.34 \times 10^4$ N/m^2 (± 0.5 psi) with an accuracy of 2%.

The general view of the experimental facility in Figure 1, from left to right, shows the storage tanks above the test section, the liquid nitrogen trailer and fill lines, and the portable gas tanks of helium and nitrogen. A close-up of the test section in Figure 2 shows the arrangement of the test section by-pass line, chill line, and a camera in position along with various pressure gages.
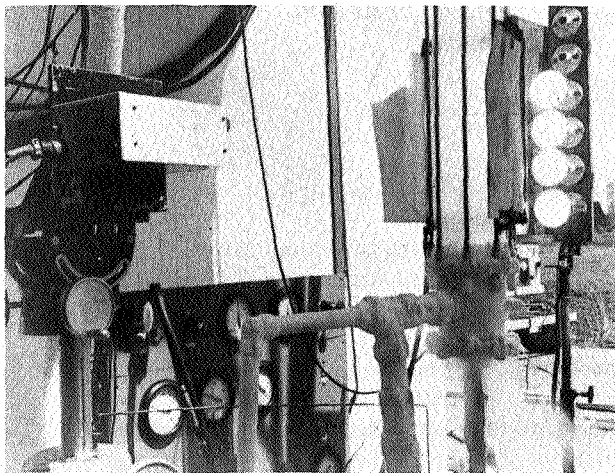

FIGURE 2. BUBBLE DYNAMICS –
EXPERIMENTAL SETUP

Because of the extent of arithmetic manipulation needed for the reduction of data, a computer program was employed. The computer program contains three main parts: reduction of experimental data, calculation of the analytical solution for the particular conditions of the experiment on an analog computer, and plotting of both theoretical and experimental data.

RESULTS

Since bubbles of different sizes will assume different shapes, the characteristic length used was one-half the average horizontal length of a bubble. Figure 3 shows the terminal velocity of helium bubbles in liquid nitrogen at 75°K (-324° F) as a function of the characteristic length (the radius of the bubble).
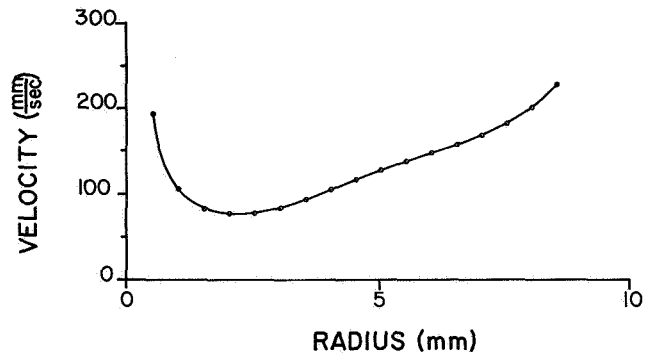
FIGURE 3. VELOCITY VS. BUBBLE RADIUS

A more generally employed presentation shows the drag coefficient as a function of Reynolds Number with a third parameter, G_1, as defined earlier, kept constant (Fig. 4).

Other experimenters have shown that up to a Reynolds Number of 70 a bubble behaves like a rigid sphere. For a Reynolds Number of 70 to 600, the hydrodynamic and surface tension forces are both important in determining the shape and consequently the drag coefficient of the bubble. As the bubble size increases, the shape of the bubble becomes flatter with a consequent rise in the value of the drag coef- ficient. For a Reynolds Number greater than 5000, surface tension plays a relatively minor role in determining the shape of the bubble; hydrodynamic forces acting on the bubble result in a mushroom shape bubble.

Since the inhouse experiments were all conducted in liquid nitrogen at one temperature with only the bubble size being varied independently, no informa- tion concerning the effect of the parameter G_1 can be derived from these data. This G_1 parameter was chosen so as to be independent of the variables in the experiments. It may be varied independently of the Reynolds number by changing either the pressure gradient or the properties of the liquid. A few

1. STOKES LAW.
2. SOLID SPHERES, LAPPLE & SHEPHERD.
3. LIVESTOCK OIL, O'BRIEN & GOSLINE.
4. MINERAL OIL, O'BRIEN & GOSLINE.
5. WATER, ROSENBERG.
6. PREDICTED FOR He GAS IN LN₂.

FIGURE 4. DRAG COEFFICIENT VS. REYNOLDS NUMBER

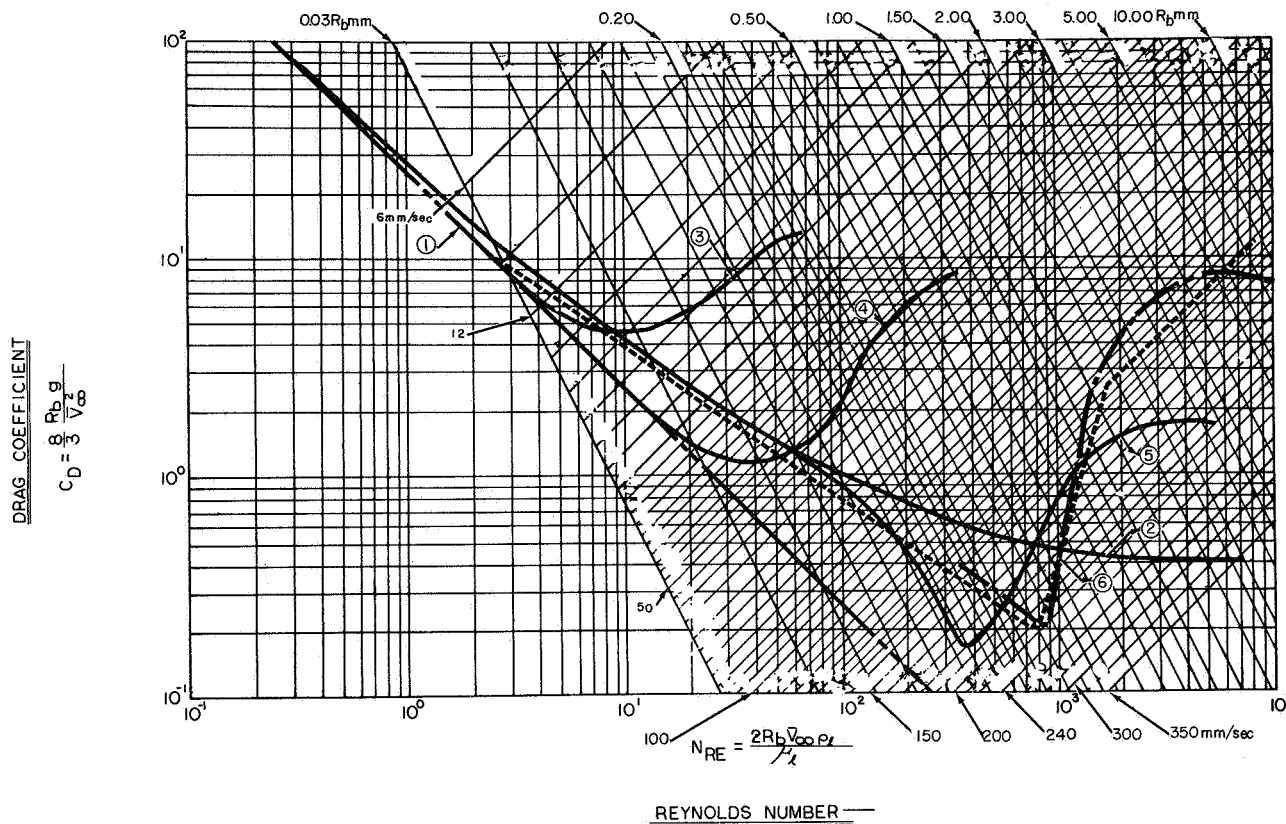generalizations appear justified, both from the expected influences of the variables incorporated in the parameter G_1 and other authors' data.

From other authors' data it appears that for very low Reynolds Numbers, the bubble behavior is almost independent of the value of the parameter G_1, the bubbles acting as rigid spheres. A puzzling aspect of the problem is the existence of a critical value of the Reynolds Number beyond which the drag coefficient of the bubble departs from that of a rigid sphere, yet the bubbles are still spherical. The available data are not sufficient to indicate definitely whether the Reynolds Number at which this break takes place is a function only of G_1 or whether the phenomenon depends upon some property of the fluids not considered in this analysis. A tentative observation is that the greater the value of G_1, the lower is the critical Reynolds Number.

Most hydrodynamics problems are concerned solely with the variation of drag coefficient with Reynolds Number for a single fluid. The form of G_1 indicates that for a specific liquid at a given temperature, changing the pressure gradient is equivalent to varying G_1. Therefore in using different liquids the same sort of information is being obtained as if the pressure gradient were varied, provided our assumption concerning the relevant physical variables is correct.

The Bond Number indicates the ability of the bubbles to remain as an entirety. As the Bond Number increases, the bubble becomes less stable. At a Bond Number of 275 (approximately 8 mm radius) the bubble was noted to break up into two or more smaller bubbles. Since the Bond Number is the force ratio of gravity to surface tension, and surface tension force decreases as the bubble radius increases,

the Bond Number should increase as the bubble radius increases. At this Bond Number, the gravitational force is much larger.

CONCLUSIONS

The motion of a gaseous bubble in a liquid can best be characterized by the use of four dimensionless numbers: The drag coefficient, Reynolds Number, Bond Number, and the fourth parameter, G_1, which for a specific liquid is proportional to the pressure gradient. The effect of G_1 on the relation between the drag coefficient and Reynolds Number is uncertain since only incomplete data are available. The Bond Number indicates the upper limit for any particular gas bubble in a liquid.

BUBBLE DYNAMICS IN VIBRATED LIQUID COLUMNS

INTRODUCTION

The experimental work in bubble dynamics was extended to the production and coalescence of bubbles by longitudinal vibrations of a liquid column filled with water and methanol.

Some parametric experimental results along with a review of the literature indicate very definite trends: higher ullage pressures require larger energy input for inception; the lower the liquid height, the higher the natural frequency of the liquid and container; and wall thickness and length/diameter ratio have a significant effect on the inception of bubble coalescence.

Several variables that must be examined closely to determine their effect are the gas content in the liquid, other properties of the liquid, properties of the container, and time dependency of inception.

Thus far, the research project is exploratory in nature and parametric tests are being run to determine general trends and to select parameters to be used for future investigations.

One of the most difficult problems encountered is the development of a non-visual method of detecting the presence of the bubble clusters. Encouraging results have been obtained during sinusoidal vibration; as the bubble clusters form they distort the sinusoidal vibration of the container by causing high frequency perturbations in the displacement of the shaker. With random vibration these high frequency perturbations are already

present even without the formation of bubble clusters, and therefore a capacitance type quality meter will probably be required to detect the clusters if they cannot be visually detected.

EXPERIMENTATION

The test program presently is investigating the effects of various variables in the formation and coalescence of bubbles in longitudinally vibrating liquid-filled elastic containers.

Initial tests were conducted using a 15.24 cm (6 in.) ID × 1.27 cm (1/2 in.) wall × 91.5 cm (36 in.) long plexiglas container with a flat bottom and an open top. This container filled with methanol was mounted on a 22 200 N force (5000 lbf) vibration exciter. A schematic is given in Figure 5.
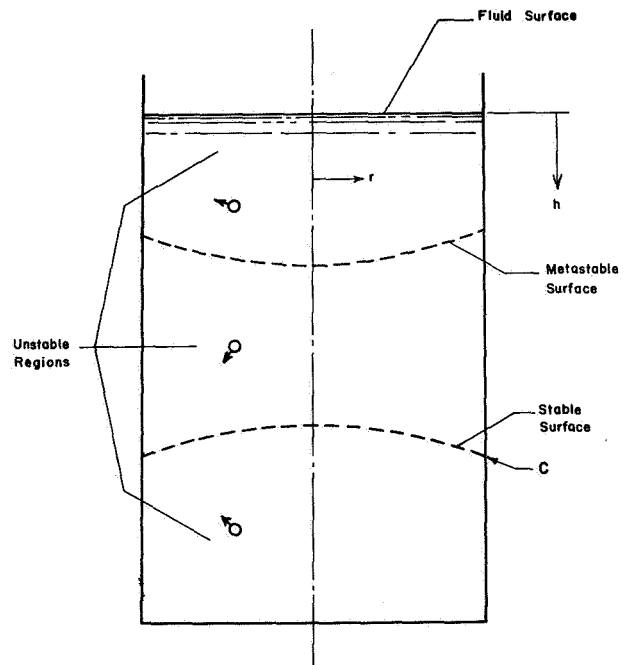
FIGURE 5. BUBBLE BEHAVIOR IN ELASTIC TANKS

The bubbles were formed in two distinct ways. The first was a surface effect where liquid droplets sloshed free of the surface; the droplets fell back through the surface and formed gas bubbles under the surface (Figs. 6 and 7). In the second method bubbles were formed at higher frequencies by the separation of dissolved gas out of the liquid, creating a very unstable condition (Figs. 7 and 8).
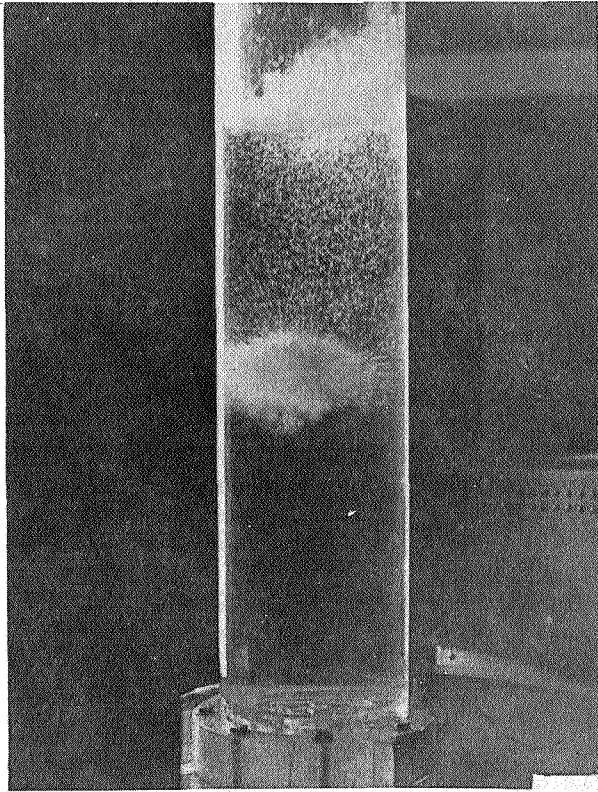
FIGURE 6. LONGITUDINAL VIBRATION -
LOW FREQUENCY (100 Hz), 10-15 g's

FIGURE 7. LONGITUDINAL VIBRATION -
INTERMEDIATE FREQUENCY (290 Hz), 20 g's

At sufficiently large vibration amplitudes, these bubbles migrated to the lower region of the column where they formed a large aggregate of bubbles. This phenomenon has been named CILIVIC (coalescence in liquids in a vibrating column). When the bubble aggregate has become sufficiently large, it rises to the surface where it remains, causing an area of foam under a severely disturbed surface.

Under random vibration (20-2000 Hz) that closely simulates the vibration that occurs during firing of large rocket engines, CILIVIC may occur in the tanks, suction lines, at the inlet to or in the propellant pumps, and even in the LOX domes.

To initiate bubble formation in a vibrating liquid, the local pressure level must be reduced to a sufficiently low value during a portion of the vibration cycle. For purposes of simplicity, it is assumed that bubbles will form at a particular location if the minimum instantaneous pressure falls below some threshold pressure value, P_T.

For pure liquids it might be expected that P_T would be close to the saturation pressure at the

liquid temperature. This idea represents a considerable over-simplification. In reality the situation is far more complicated because the threshold pressure required to produce bubbles is dependent upon frequency, surface tension, dissolved gas properties, and a number of other factors.

The condition for inception of bubble formation in the system is obtained in the following equations:

$$G_T = \left[1 + \left(\frac{P_u}{pgL} \right) \left(1 - \frac{P_T}{P_u} \right) \right] \left(\frac{\Omega}{\tan \Omega} \right) \qquad (1)$$

and

$$G_T \approx \left[\frac{\pi}{2} + \left(\frac{P_u}{pgL} \right) \left(1 - \frac{P_T}{P_u} \right) \Omega \right] |\cos \Omega|. \qquad (2)$$

Where,

G_T threshold acceleration level required to produce bubbles

P_u ullage pressure
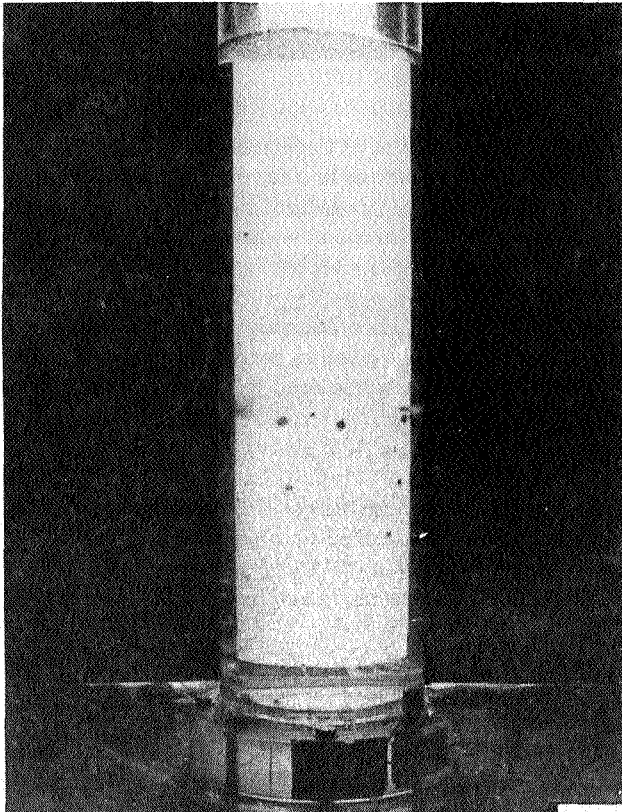
FIGURE 8. LONGITUDINAL VIBRATION –
HIGH FREQUENCY (450 Hz), 30 g's

P_T threshold pressure required to produce bubbles

ρ fluid density

g acceleration of gravity

L length of the liquid column

Ω dimensionless angular frequency, $\dfrac{\omega L}{c}$.

G_T represents the threshold acceleration level required to produce bubble formation. Equation (1) gives the acceleration level required to produce bubble formation at the bottom of the cylinder for $G_T > 1$ when $\Omega < \dfrac{\pi}{2}$, while equation (2) gives the level required to produce bubbles close to $\dfrac{x}{L} = \dfrac{\pi}{2\Omega}$ when $\Omega > \dfrac{\pi}{2}$ (provided that $\dfrac{G_T}{|\cos \Omega|} >> 1$).

RESULTS

Longitudinally vibrated liquid columns exhibit a variety of characteristics; however, these can be broken down into two distinct phenomena. The first is a surface effect where gas is entrapped in the fluid and small bubbles coalesce into a much larger pulsating aggregate at the bottom of the tank. The aggregate periodically disintegrates or plodes causing a severe surface disturbance (Fig. 6). The second effect is a separation of the gas in the liquid at discrete layers located at what appears as pressure nodes of the wave fields (Figs. 7 and 8).

At random vibration such as that developed during firing of large rocket engines, coalescence in a liquid vibrating column (CILIVIC) can occur at the inlet to the propellant pumps or in the pumps themselves and in the LOX domes, and in the long suction lines or elbows. At times CILIVICS may even be helpful.

A parametric test program is presently being initiated to investigate the effects of some of the variables in the formation and coalescence of bubbles in longitudinally vibrating liquid filled elastic containers.

The initial tests were conducted using a 15. 24 cm (6 in.) ID × 1. 27 cm (1/2 in.) wall × 91. 5 cm (36 in.) long plexiglas container with a flat bottom and an open top. This container was mounted on a 22 200 N force (5000 lbf) vibration exciter and filled with methyl alcohol to a height of 50. 8 cm (20 in.) above the tank bottom. When the container was vibrated at low frequencies (40 to 150 Hz), the surface would begin to slosh. As the acceleration was increased, the surface slosh became violent, and droplets of the fluid were thrown free of the surface. When these droplets fell back through the fluid surface, they formed gas bubbles under the surface. Buoyancy then caused these bubbles to return to the surface. As the acceleration level was increased further, however, the bubbles would migrate to the bottom of the container instead of floating upward. As the number of bubbles within the liquid increased, the migration of the bubbles from the surface increased until a large aggregate of bubbles formed within the fluid. Although a quasi-steady state was reached, this aggregate would continue to grow very slowly and with this growth it would finally reach the surface. The migration of small bubbles would again start and form another cluster within the fluid.

When the container was vibrated at the higher frequencies, the large sloshing motion of the free surface was absent. As the acceleration level was increased, only standing waves were visible on the surface until, with a sharp cracking noise, bubble clusters formed at discrete layers in the tank. These clusters moved rapidly and violently around in the container, and as some went to the surface,

19

new clusters formed. The clusters rotated at a rather high speed. When a cluster neared the free surface, the spinning motion made a surface spray above the bubble.

The parametric studies to some degree have determined the effect of the ullage pressure, the liquid height, and the time of imposed vibration on the formation of the bubble clusters. The ullage pressure in these containers was varied. The time in which bubbles form depends on the acceleration level. For example, as is shown in Figure 9, an imposed vibration of 12 g's at 110 Hz will cause a bubble cluster to form after 120 seconds. The size of the bubble and bubble clusters is related inversely to the frequency of vibration (Fig. 10).
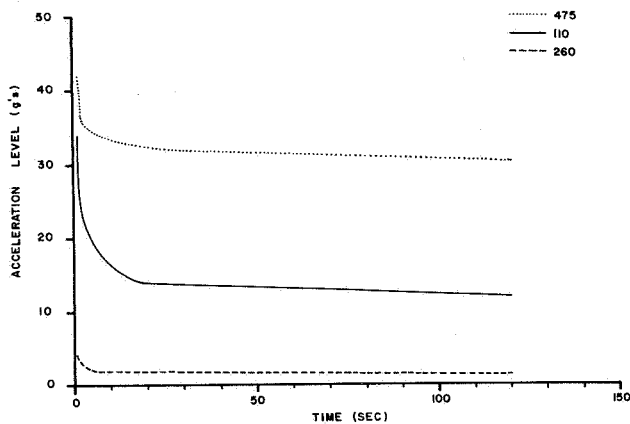

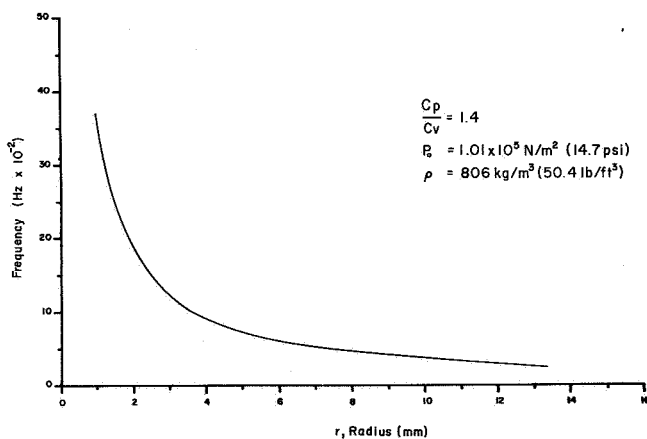FIGURE 9.   VARIATION OF BUBBLE FORMATION WITH DWELL TIME

FIGURE 10.   BUBBLE RADIUS VS. FREQUENCY

TWO-PHASE FLOW

INTRODUCTION

The investigation of two-phase fluid flow phenomena is important in answering questions on the venting of cryogenic propellant tanks while in space, chilling of transfer and engine propellant lines, and generally advancing the technology in launch vehicle design.

During the past two decades an exponential increase in efforts has been expended to describe the various phenomena associated with two-phase (gas-liquid) flow. Much of this effort has been directed toward application for nuclear reactor design. Consequently, most experimental data have been gathered using steam-water mixtures. Recently, the development of vehicles required data on the behavior of two-phase fluid flow with cryogenic systems. This work covers inhouse investigations with cryogenic fluids.

Two-phase fluid flow exhibits a critical flow phenomenon analagous to that of a compressible fluid. When a compressible fluid flows through a restriction, such as a converging nozzle, the fluid velocity is increased by decreasing the downstream pressure until a limiting or critical velocity is attained in the throat of the restriction. This limiting velocity is coincident with the speed of sound in the fluid, and the downstream pressure producing the critical velocity is the critical pressure.

In the divergent section of the nozzle the velocity may then become supersonic for some distance until a shock wave reduces the velocity to a subsonic value, or the velocity may start decreasing as soon as the fluid undergoes its maximum velocity at the minimum cross-sectional area of the restriction. The governing equations may be derived from the equations of fluid motion, the energy equation and the equation of continuity.

Two-phase critical flow is not as readily analyzed as is compressible fluid flow because of thermodynamic metastability and flow pattern considerations. Analyses based on a homogeneous fluid in thermodynamic equilibrium and the various two-phase patterns yield good results in long tubes where no large amount of thermodynamic metastability exists. Analyses assuming no exchange of mass from one phase to the other are also used to predict the critical two-phase flow rate.

EXPERIMENTATION

Experiments were conducted to determine the critical flow rate of two-phase nitrogen. All data were collected using a stagnation pressure of 0.172×10^6 N/m^2 (25 psia). To assure critical flow, the downstream pressure was decreased until further decreases in downstream pressure produced no change in flow rate. This pressure was then used as the critical receiver pressure and experiments were conducted using a downstream pressure substantially below this apparent critical pressure. The fluid was not observed visually within the experimental apparatus.

The experimental apparatus (Fig. 11) consisted of a 4.75 cm (1.87 in.) inside diameter × 86.4 cm (34 in.) long horizontal cylindrical plenum chamber. The two-phase fluid enters the plenum through a 1.07 cm (0.42 in.) diameter square-edge orifice and exits through a 2.87 cm (1.13 in.) diameter square edge orifice into a vacuum chamber. All results presented are for the 1.07 cm (0.42 in.) diameter orifice. Two-phase fluid flow was generated upstream of the plenum by mixing liquid and gaseous nitrogen.

RESULTS

Thirty-six experiments were conducted that covered the entire quality range. Experimental mass flow rates, ζc, are plotted versus stagnation quality in Figure 12, and are compared to the predicted flow rates.

On comparing the experimental data to the various predictions, the experimental data were most closely approximated by the Frozen Equilibrium Model. This is indicative of a large amount of thermodynamic metastability while flowing through the orifice. Many references on critical two-phase fluid flow indicate that the assumption of thermodynamic equilibrium should not be invoked in restrictions with length-to-diameter ratios of less than ten, and the experimental data confirm this assumption.

Most analytical predictions overpredict the critical mass flow rate for low quality fluids. This phenomenon was noted on comparing the experimental data to predictions. Stratified flow probably existed in the experimental apparatus, and this digression from the proposed models may explain the difference between this experimental data and other predictions.
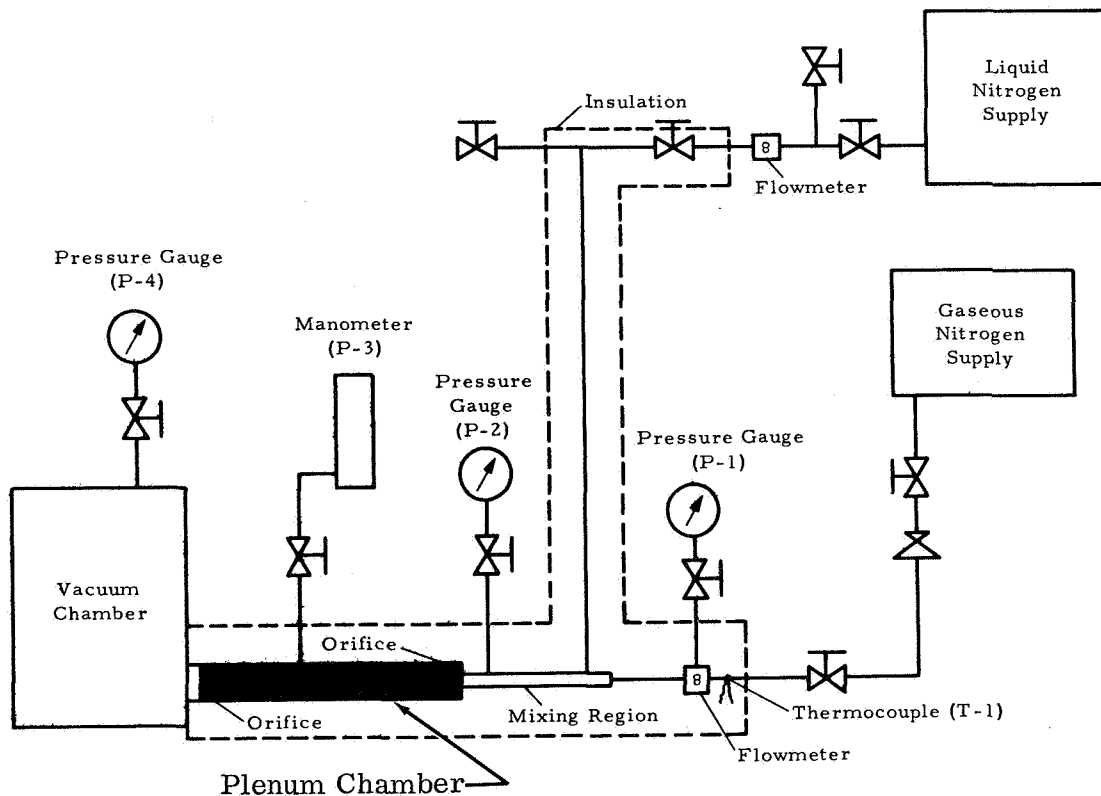

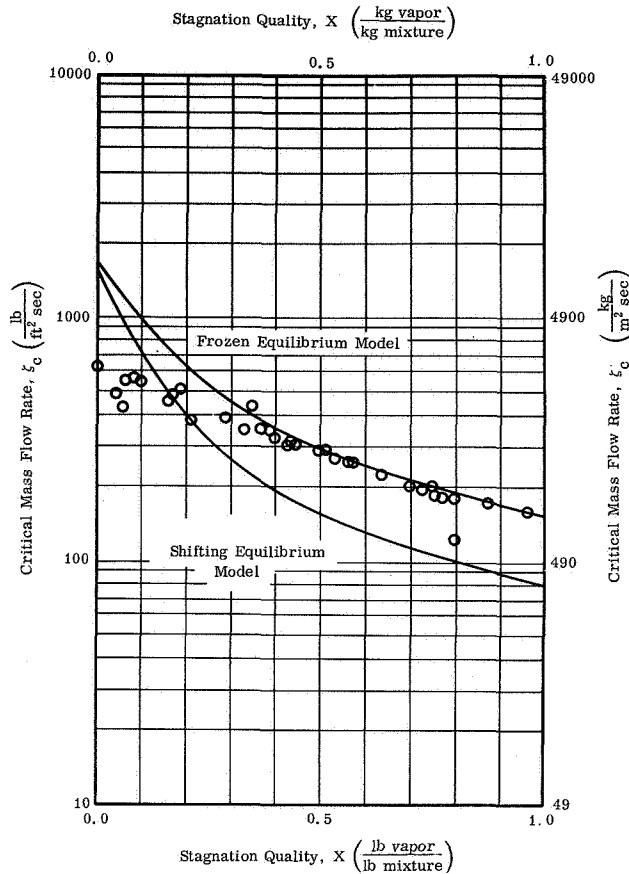FIGURE 11. SCHEMATIC OF TWO-PHASE FLOW

Stagnation Quality, X $\left(\frac{\text{kg vapor}}{\text{kg mixture}}\right)$

FIGURE 12. CRITICAL MASS FLOW
RATE VS. STAGNATION QUALITY

Stagnation Quality, X $\left(\frac{\text{lb vapor}}{\text{lb mixture}}\right)$

various Reynolds Numbers and at several radial
positions in the pipe. The velocity distributions
were measured and from them the mean and the
variance were established. In addition, the dis-
tributions obtained are illustrated and reveal the
skewness as affected by the radial position in the
pipe. The results obtained provide new information
on turbulent liquid flow.

Previous investigators have used eddy diffusion
data to determine inferences concerning the velocity
distribution. Foreman, Lewis and George in an
earlier report described the technique for using the
laser for Doppler measurement in fluids.

APPARATUS

The velocimeter system is composed of three
separate elements (Fig. 13). A liquid flow loop
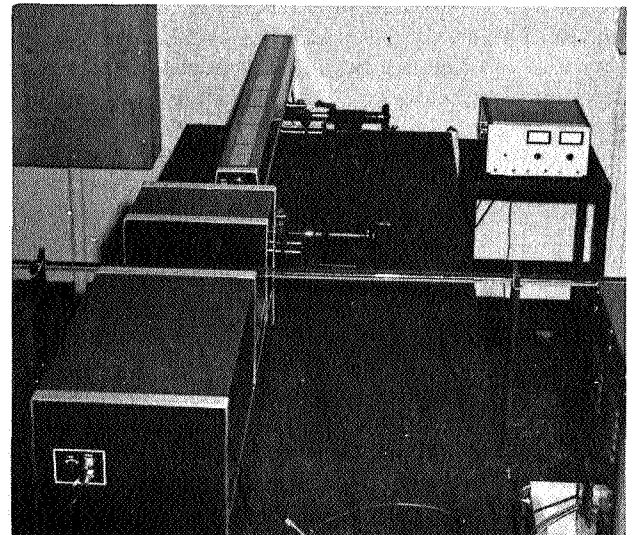
FIGURE 13. VELOCIMETER SYSTEM

provides a constant bulk flow through a glass tube
of 2.2 cm inside diameter. The driving force for
flow is obtained from a pump or from an elevated
tank. The flow system is standard and thus is not
described. A gas laser is used with associated
optical equipment and is referred to as the optical
system. The third part of the system is the elec-
tronics that convert the optical measurement into
a useable electronic signal.

The Optical System schematic is shown in Figure
14. A He – Ne gas laser was used to provide a beam
of coherent light that was directed through the glass

VARIATION OF STATISTICAL THEORY
OF TURBULENCE

INTRODUCTION

The various techniques used to measure the
velocity of liquids in turbulent flow have traditionally
involved the use of some device protruding into the
flow stream. Most devices of this type have in-
sufficient response, hence turbulent fluid flow meas-
urements were difficult. In this investigation a
beam of light measures the velocity of the fluid by
application of the Doppler effect. Furthermore, an
electronic system was developed to measure the
velocity distribution at a point, and to have a fre-
quency response believed to be well above that re-
quired.

The purpose of this investigation is to define the
velocity distributions for liquids in turbulent flow for

tube as shown in Figure 15. The focal point was located at six different positions throughout the
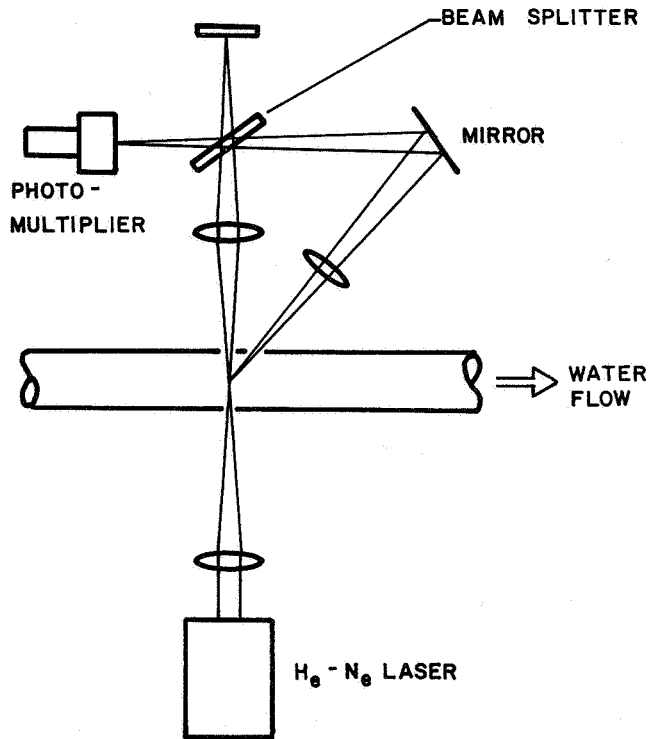

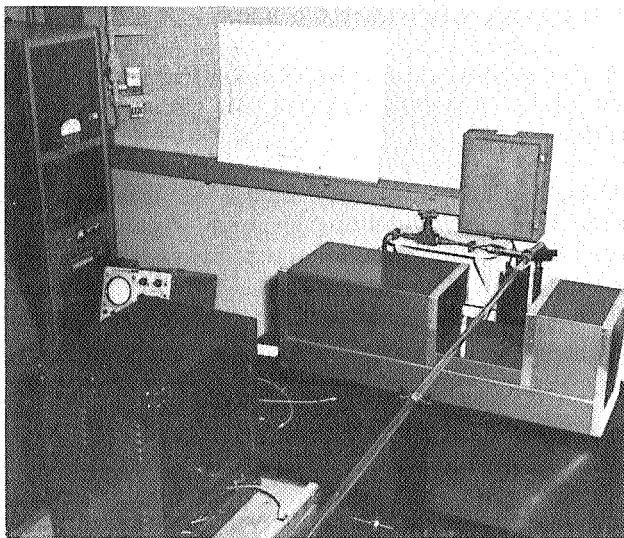FIGURE 14. OPTICAL SYSTEM SCHEMATIC

FIGURE 15. VELOCIMETER SYSTEM

course of the investigation. Light is scattered from the focal point by small particles in the water. A lens arranged at a known angle was aimed to receive the light scattered at that angle. This light differs in frequency from the parent beam because of the Doppler effect produced by the motion of the solids in the water. These two light beams when recombined on the cathode of a photomultiplier tube produce a heterodyne signal. For the studies described in this paper, the heterodyne frequency was less than 500 kHz. The optical system was mounted on a moveable platform separate from the glass tube. This feature permits traversing the fluid within the pipe. The optical arrangement measured the longitudinal component of the velocity at the focal point. Concisely, the optical system provides a heterodyne signal that is directly proportional to the longitudinal component of the fluid velocity at the focal point.

RESULTS

Velocity distributions were obtained at the center line of the tube for four Reynolds Numbers, and velocity profile measurements were made at five radii. Figures 16 and 17 show typical point velocity
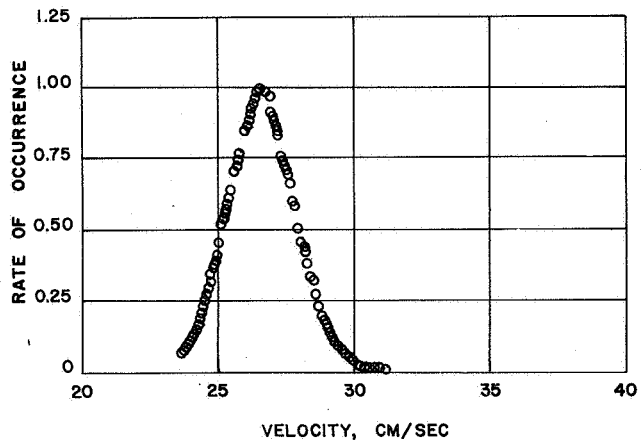

FIGURE 16. POINT VELOCITY DISTRIBUTION, $N_{Re} = 4605$

distributions obtained at Reynolds Numbers of 4605 and 9310. The same general shapes result at other Reynolds Numbers with a shift in velocity and variance. Since the velocity is directly proportional to the heterodyne frequency, the velocity distribution functions are derived directly from the heterodyne frequency distributions.
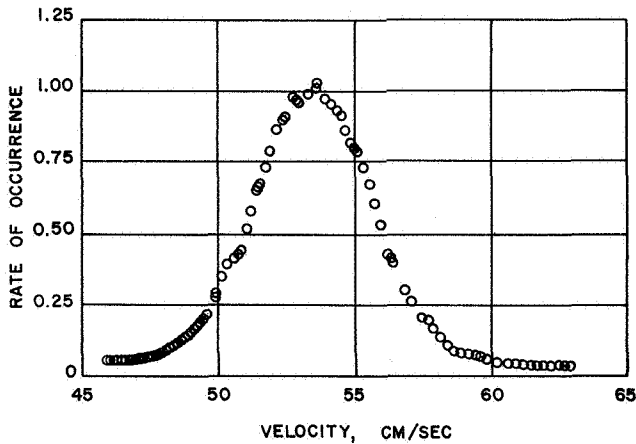
FIGURE 17. POINT VELOCITY DISTRIBUTION,
$N_{Re} = 9310$

Figure 18 shows a velocity profile obtained by plotting the mean velocities measured at several radii within the pipe. The continuous curve represents Nikuradse's data and in general there is very close agreement. Measurements closer to the wall are possible but were inconvenient because of the changes required; hence, they were not attempted during this investigation.

CONCLUSIONS

The measured velocity distribution function is verified for both its mean value and the variance. The mean velocities were verified with existing data by Nikuradse and a profile in radius of the mean values is shown in Figure 18.

The shape of the measured distribution function agreed with concentration gradients measured near the source. The measured variances were verified by calculating the corresponding eddy diffusivities and comparing with the measured eddy diffusivities.

The general velocity distribution function was established with data and a statistical derivation.
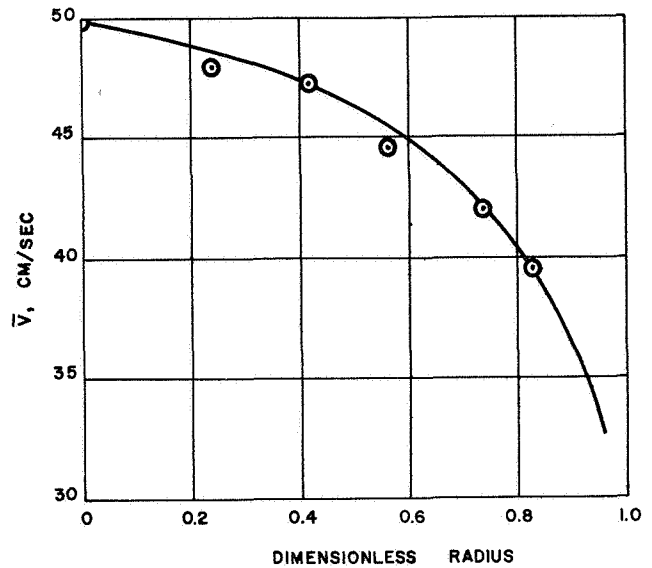
FIGURE 18. MEAN VELOCITY PROFILE,
$N_{Re} = 8510$

The general velocity distribution function accounts for the increase in skewness in the distribution function that appears when the position of measurement approaches the radius of the pipe wall. Sufficient velocity data are not yet available near the wall to completely confirm the general velocity distribution function; however, the existing data show good agreement. Further, the velocity distribution as measured near the center of the pipe is a normal distribution which is in agreement with the derived general velocity distribution function.

It was established that the distribution function and the variation in radius agreed with statistical concepts.

Using statistical concepts of fluid mechanics as shown by papers in the bibliography, it is possible to derive the function describing the variation of the variance as a function of the radius. This function is verified by the data obtained.

BIBLIOGRAPHY

1. Blount, D. H.; Fritz, C.; and Ponder, C. A.: Bubble Coalescence in a Longitudinally Vibrated Liquid Column. Part I - NASA TMX-53180, 1964.

2. Campbell, H. M., Jr.; and Overcamp, T. J.: Critical Flow Rate of Two-Phase Nitrogen. Proceedings of the Southeastern Symposium on Missiles and Space Vehicles Sciences Sponsored by the American Astronautical Society, Dec. 5, 6, 7, 1966, pp 46-1 to 46-11.

3. Campbell, H. M., Jr.; and Head, R. R.: Analysis of Fluid Conditions in the Discharge Line of a Cryogenic Container Undergoing Self-Pressurized Draining. Proceedings of the Southeastern Symposium on Missiles and Space Vehicles Sciences, Sponsored by the American Astronautical Society, Dec. 5, 6, 7, 1966, pp 47-1 to 47-12.

4. Campbell, H. M., Jr.: Fluid Quality in a Self-Pressurized Container Discharge Line. NASA TMX-53330, 1965.

5. Fritz, C.: Study of Gas Bubble Dynamics. Part I - IN-R-P& VE-P-64-5, 1964.

6. Fritz, C.: Study of Gas Bubble Dynamics. Part II - IN-R-P& VE-P-65-13, 1965.

7. Overcamp, T. S.; and Schoenhals, R. J.: Pressure Distribution and Bubble Formation Induced by Longitudinal Vibration of a Flexible Liquid-Filled Cylinder. NASA TMX-53353, 1965.

8. Tomme, W. J.; and Welch, N. E.: Study of Turbulence with Data Obtained with a Laser Velocimeter. A.I.A.A. Bulletin, Vol. 2, No. 11, Jan. 1967.

9. Tomme, W. J.; and Welch, N. E.: Study of Turbulence with Data Obtained with a Laser Velocimeter. A.I.A.A. Conference, New York, Jan. 22-26, 1967.

10. Tomme, W. J.; and Welch, N. E.: Correlation of Velocity Distribution in Functions for Turbulent Pipe Flow. ASME-AICh. E Conference, August 1967.

LARGE ENGINE TECHNOLOGY

By

Keith B. Chandler

SUMMARY

The Nation's present launch vehicles should suffice for space exploration objectives for the next 10 to 15 years. A sound technological base is being prepared now for future missions that will require additional performance.

To find an improved engine for upper stages, two primary paths are being pursued. One is an extension of the capability of the Bell-nozzle engine (by increased chamber pressure); the other is the use of unconventional geometry (e.g., annular combustion chamber and aerospike nozzle). Design studies and certain discrete component and sub-assembly tasks offer the required technology base, using guidelines from systematic studies of advanced vehicles and missions.

Though the requirement for a new launch vehicle larger than present ones is not urgent, a limited effort consisting of two major and one minor concepts is being considered. One concept is the plug multi-chamber, a cluster of modular engines mounted on the periphery of the base of the vehicle and surrounding a truncated plug. Another concept is a toroidal chamber around the periphery of the base of the vehicle and exhausting onto a truncated plug (aerodynamic spike). The other possibility is a group of modular toroidal engines clustered in the conventional manner. Analytical and limited experimental investigations are being conducted for future propulsion systems.

INTRODUCTION

The Nation's present launch vehicles possess a massive capability to launch large payloads into earth orbit and lunar trajectories. Extensive use of this huge capability is planned by having larger payloads and more ambitions missions than originally conceived. Thus the immediate objective is to further develop spacecraft and payloads for greater benefits. The need for new launch vehicles is not so urgent, but is certainly included in plans for the future. The Nation's present stable of launch vehicles (SATURNS, ATLASES, THORS, and TITANS) should accomplish the space objectives for the next 10 to 15 years. This does not exclude a need for change. Specific missions will dictate modification of available hardware, and eventually there will be missions requiring additional performance.

To find an improved engine for upper stages, we now pursue two primary paths in our engine technology efforts: one is an extension of capability in the bell-nozzle engine (by increased chamber pressure) for higher thrust and higher specific impulse in the current dimensional envelope; the other is the use of unconventional geometry (e.g., annular combustion chamber and aerospike nozzle). The actual performance (specific impulse) of these two configurations is still to be demonstrated; but of even greater importance than performance are the vehicle/engine interface considerations such as simplicity, commonality (usefulness in more than one stage or application), throttleability and service life. Based on the technology conducted on these configurations to date, the data available are insufficient to make a selection between the two at this time.

Since there are no firm mission requirements for an advanced engine, a development program is unwarranted. There is, however, a need for establishing a technological base from which a development program could be undertaken. Certain discrete component and sub-assembly tasks offer this technology base, and systematic studies of advanced vehicles have provided guidelines for an advanced engine. The values in Table I are being used for the component investigations.

ADVANCED ENGINE, BELL

The basic effort in the high-pressure-bell configuration is the Advanced Engine Design Study (Bell)[1]. This is a comprehensive program aiming for a specific definition of an advanced bell-engine in the 1.56 MN thrust (350,000 lb thrust) class. Special attention in this program is on the requirements identified in the studies of uprated

TABLE I. ADVANCED ENGINE GUIDELINES

Thrust	1.40 to 2.22 MN (315,000 to 500,000 lb, in vacuum)
Thrust Range	Main Stage and Idle Mode
Specific Impulse, sec	450+
Mixture Ratio, o/f	5 to 7
Dia (Max)	2.03 to 3.56 m (80 to 140 in.)
Length (Max)	3.38 to 3.86 m (133 to 290 in.)
NPSH Fuel	0 to 79.3 m (0 to 260 ft)
NPSH Oxidizer	0 to 21.3 m (0 to 70 ft)

future launch vehicles and the Reusable Orbital Transport. The objectives are selection of an engine cycle and integration of specific components for the best over-all balance of performance, operational characteristics, dependability, and installation flexibility. For use in vehicle studies, parametric engine performance data and an estimate of development cost and time are being prepared, and critical engine components or advanced concepts that should be verified experimentally are being identified. One of the objectives of the Advanced Engine, Bell (AEB) design is an engine suitable for several installations. This objective implies that the design must avoid concepts that would (1) burden the vehicle with operation-restricting features to compensate for limited thrust response, (2) require additional systems for engine preconditioning, or (3) impose restrictions on vehicle-command sequencing.

The cycle selected is one known as the "preburner" cycle (Fig. 1). Most of the hydrogen and some of the oxygen is burned in the preburner. The resulting low-temperature gas approximately 922° K (1200° F) drives the two turbopumps and then flows into the main chamber, where the hot, hydrogen-rich gases are mixed with the balance of the oxygen and hydrogen to complete combustion. The chamber pressure of the preburner is approximately 3.44×10^7 N/m^2 (5000 psi); the pressure in the main chamber is approximately 2.06×10^7 N/m^2 (3000 psi).

The concept illustrated includes an extendible nozzle cooled by hydrogen flowing through a tube bundle and "dumped" (exhausted) through tiny nozzles at the exit of the main nozzle. The specific performance of this warm hydrogen is almost equal
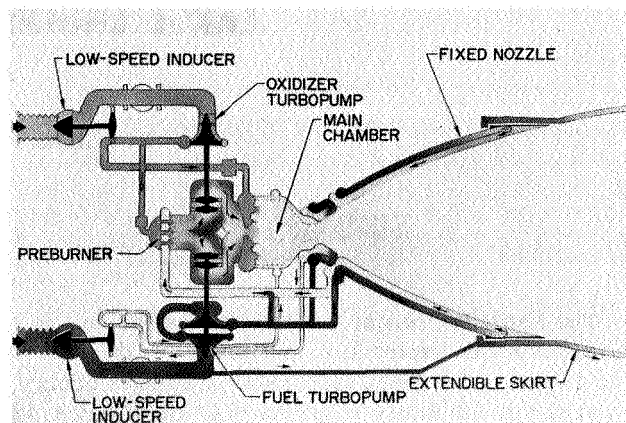

FIGURE 1. SCHEMATIC OF ADVANCED ENGINE, BELL

to that of the gases from the main chamber. A full-scale mock-up is pictured in the right side of Figure 2, with the nozzle in the retracted position. In Figure 3 the nozzle is in the extended position. In
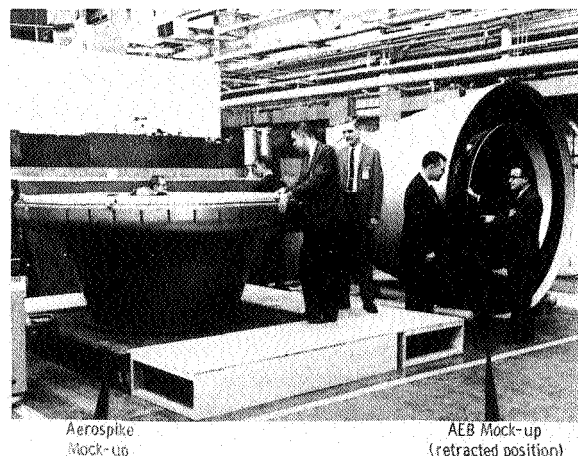

FIGURE 2. ADVANCED ENGINE, BELL MOCK-UP (RETRACTED POSITION)

application, the nozzle is stored in the retracted position to reduce interstage length. In a sea-level-launch application, the nozzle would be in the retracted position at launch, and extended at the appropriate altitude to gain higher performance from the higher expansion ratio (Fig. 4). When used in an upper stage, the nozzle would be extended after the stages are separated and before ignition of the engine.
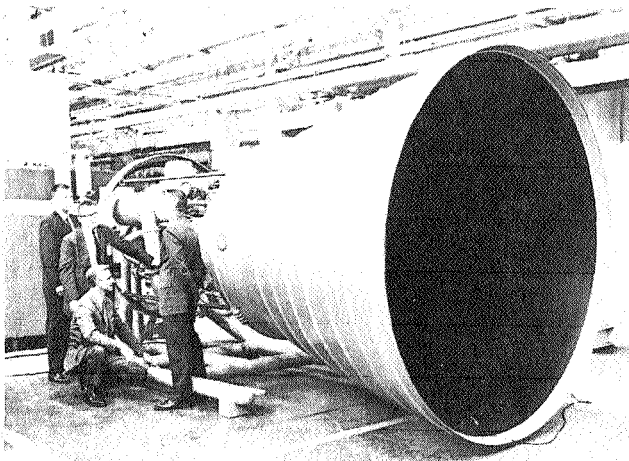
FIGURE 3. ADVANCED ENGINE, BELL
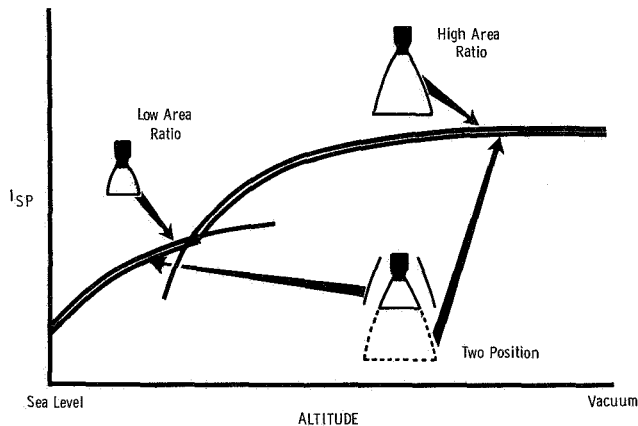MOCK-UP (EXTENDED POSITION)

FIGURE 4. INTERCHANGEABLE NOZZLES
(I_{sp} VS ALTITUDE)

To yield the desired high performance, the
Advanced High-Pressure Bell design must incorpo-
rate technological advances in the design of com-
ponents and systems. Though the engine cycle and
the detailed definition of what advanced concepts
and components will be included are not yet specific,
some general requirements are known, particularly
the advantages of higher pressure levels. Timely
development of components to fit these requirements
will give confidence that the concept is sound and will
generate information for arriving at an optimum,
component-integration scheme. The design,

fabrication, and testing of a breadboard, high pres-
sure, liquid hydrogen pump is in progress to verify
performance characteristics desirable for advanced
rocket engines [2] .

The pump fits a breadboard engine in the
1. 56 MN thrust (350, 000 lb thrust) class, as out-
lined previously. Already, some 35 tests have been
run on this pump (Fig. 5) and the maximum dis-
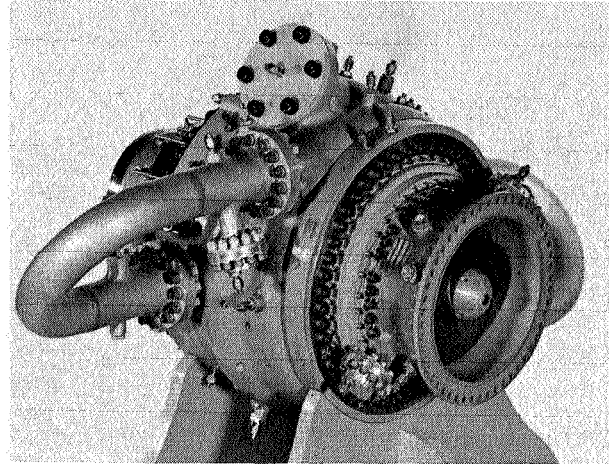charge pressure reached has been slightly more than

FIGURE 5. HIGH PRESSURE
LH$_2$ PUMP

$3. 51 \times 10^7$ N/m^2 (5, 100 psi) , the highest known
pressure yet for pumping hydrogen. Initial testing
revealed problems in volute strength and the balance
piston. These problems were solved by a redesign
of the volute tongues and the use of leaded-bronze
inserts. Also, the contractor had a problem with
non-synchronous, hydro-mechanical oscillations
which caused failure of the end bearing. This was
corrected by replacing the ball bearing with a roller
bearing and increasing the spring rate of the bearing
mount. Pump efficiency is about 8 to 10 points
lower than the design specified. It is believed that
the efficiency can be brought up to the design value
by the use of a shrouded impeller, but a change of
such magnitude is not within the scope of this in-
vestigation.

Although this program has had a number of dif-
ficulties and there have been some spectacular failures
in testing, the results achieved have been very
encouraging. A high probability for the occurrence
of failures was allowed in plans for extending the

limits of existing technological capability. The information obtained will be very useful if a development program is begun.

A companion task is the design, fabrication, and test of a liquid oxygen, high-pressure pump [3] (Fig. 6) also compatible with the breadboard engine
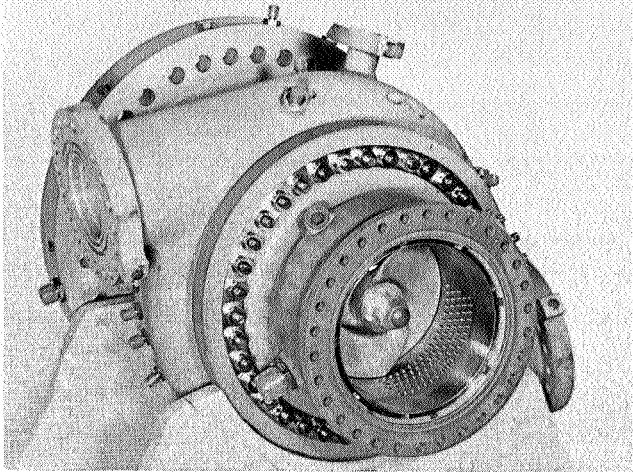

FIGURE 6. HIGH PRESSURE LOX PUMP

system outlined previously. This program was started approximately one year after the hydrogen pump, and testing has just begun. Early design and testing was very successful. Besides the requirements of thrust, mixture ratio, specific impulse, throttleability and pressure rise, the pump must be stable over the widest possible range of flow and head rise; it must provide pressure-oscillation-free operation; it must be useable in an engine cycle containing either a gas generator or a preburner; and it must operate with minimum before-start temperature conditioning.

Axial and centrifugal designs were considered for both pumps. Designs were evaluated and compared for suitability to alternative engine cycles, vehicle requirements, temperature-conditioning requirements, and development risks. Primarily because of the throttleability requirements (down to 3% of nominal thrust), the centrifugal configuration was selected in both cases.

ADVANCED ENGINE, AEROSPIKE

The other major candidate for the advanced cryogenic rocket engine is the toroidal,

aerodynamic-spike thrust-chamber. The upper illustration of Figure 7 is a conventional spike

CONVENTIONAL SPIKE NOZZLE
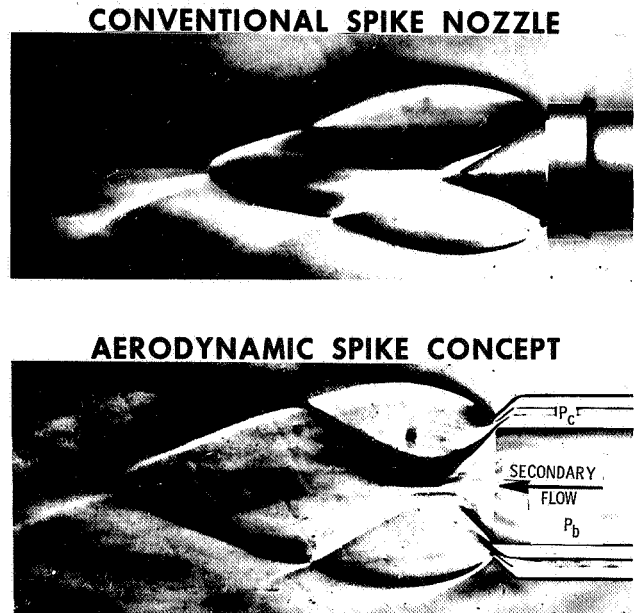

AERODYNAMIC SPIKE CONCEPT

FIGURE 7. CONVENTIONAL SPIKE AND AERODYNAMIC SPIKE COMPARISON

("plug") nozzle, with a physical plug. In the aerodynamic spike concept, the physical plug is simulated by an aerodynamic flow of warm gas. The primary gas comes from the main combustion chamber, the secondary flow from the gas used to drive the pump turbine(s).

The aerospike has the capability for "altitude compensation" so useful for sea-level-launch applications. Altitude compensation is possible by the decrease in ambient pressure associated with increased altitude; this permits the primary flow to expand (see free jet boundary, Fig. 8). Considerable cold flow data have been gathered to determine the performance of this concept, and these have been verified by hot-firing tests (Fig. 9). A conceptual design of such an engine system is in Figure 10 [4].

An outstanding feature of the Advanced Engine, Aerospike (AEA) concept is the high performance possible from a relatively short nozzle at both sea-level conditions and vacuum conditions. High performance is achieved by efficient combustion and reaction at the largest area ratio permitted by the envelope, augmented by injection of gases into the base of the spike-nozzle to amplify the base pressure, thus providing base thrust augmentation without
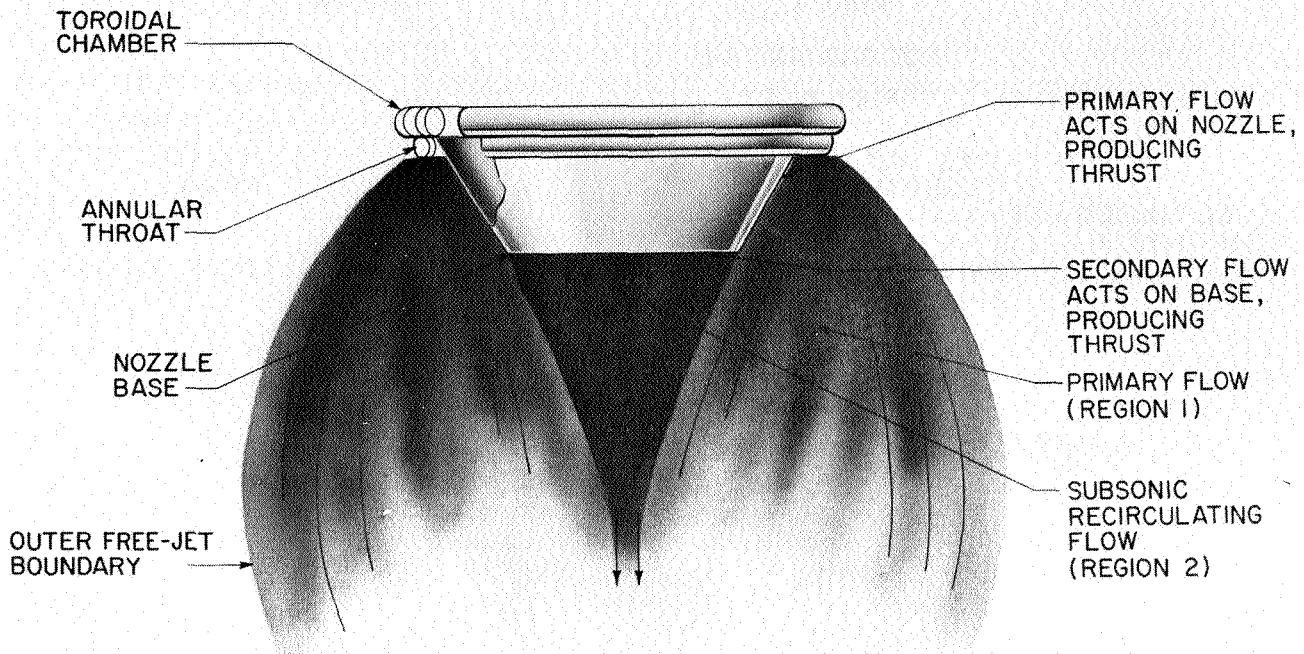
FIGURE 8. AERODYNAMIC SPIKE FLOW FIELD UNDER ALTITUDE CONDITIONS
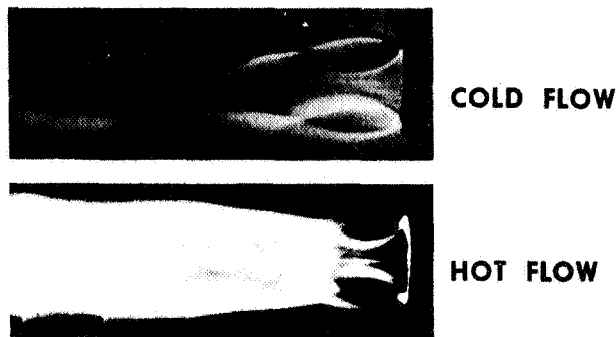

COLD FLOW

HOT FLOW

FIGURE 9. AERODYNAMIC SPIKE COLD
FLOW AND HOT FLOW COMPARISON

changing the performance of the spike nozzle. Experimental data indicate that for a given nozzle geometry and operating conditions such as chamber pressure and mixture ratio, engine specific impulse is a function of the ratio of secondary-to-primary flow. Propitiously, the optimum secondary flow is nearly equal to that which would normally be provided from the turbine exhaust.

At low altitudes, the base pressure does not drop below ambient, thus removing the characteristic, negative-pressure term of the conventional bell nozzle.

Although the ultimate configuration of the toroidal aerospike engine has not been determined at this time, certain features peculiar to the concept can be and should be investigated, particularly the thrust chamber and the fluid dynamics associated with the starting phase of the operational cycle.

A full-scale, 1.11 MN thrust (250,000 lb thrust) toroidal aerospike chamber is being built and tested (Fig. 11) in a program called "System and Dynamics Investigation" [5]. The objective is to identify the structural and dynamics problems rather than to provide the solution for problems caused by the hardware used. The approach includes analysis, priming, and cold-flow tests, segment and ignition tests, and breadboard thrust-chamber tests. Mainstage and start-transient tests will be made on a pressurized test stand with programmed main valve controls to simulate system dynamics transients. A complete dynamic description of the thrust chamber will be obtained for use in extensive system analysis. The key difference between a hydrogen engine and a hydrocarbon engine is the behavior of the compressible fuel in the thrust chamber cooling jacket. When a chamber is cooled with hydrocarbon fuel such as RP-1 or other nearly incompressible fluids, heat
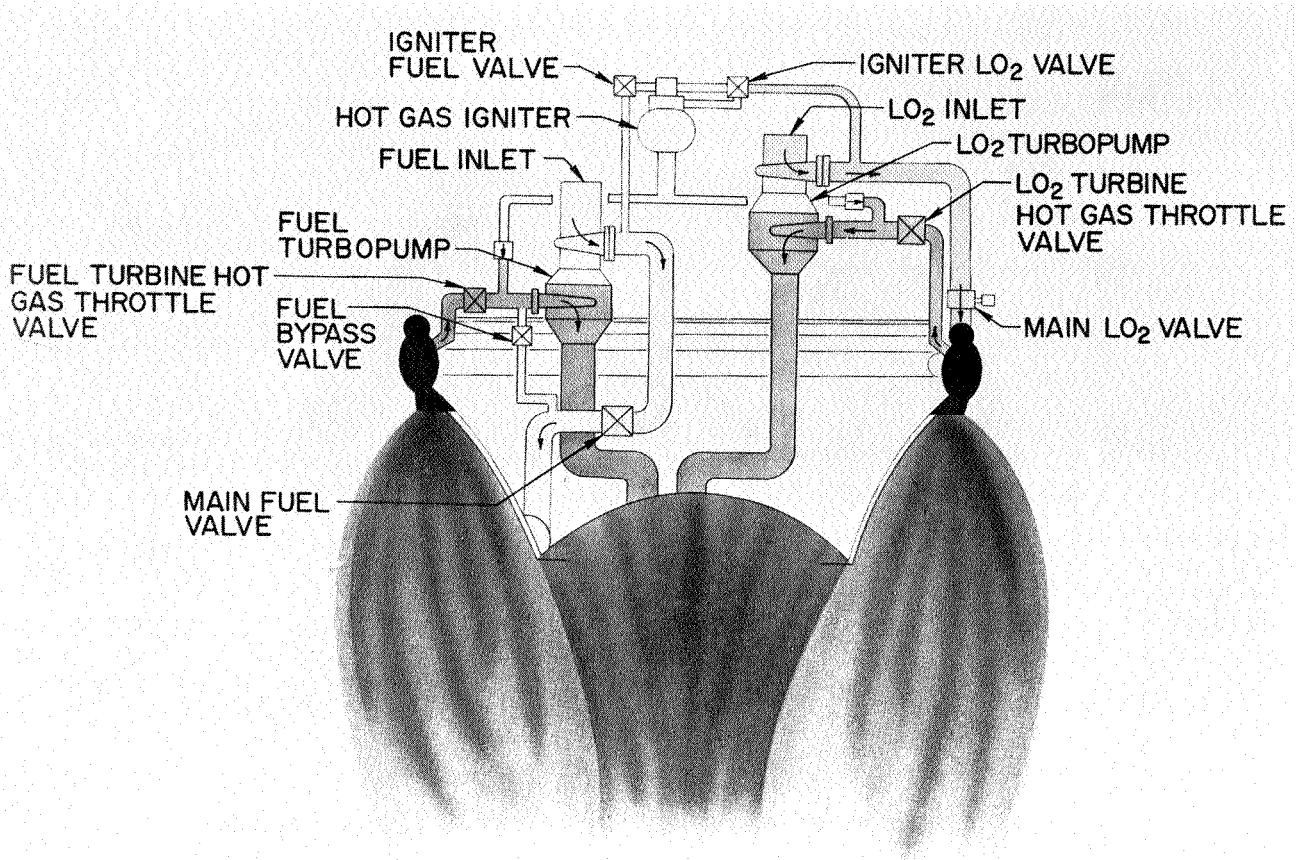
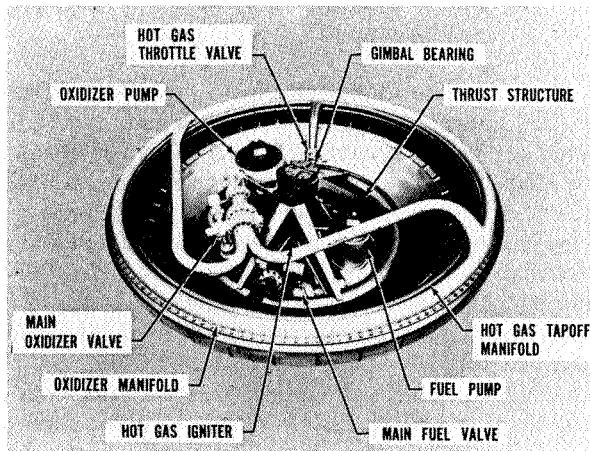FIGURE 10. SCHEMATIC OF ADVANCED ENGINE, AEROSPIKE

FIGURE 11. AEROSPIKE MOCK-UP

transfer to the liquid has no appreciable effect on the flow process. On the other hand, a hydrogen-cooled thrust chamber behaves in a more complex

manner because heat transfer has a direct effect on the flow process and the pressure drop. The hydrogen enters the cooling tubes as a liquid and emerges as a gas. At low operating levels, tube-bundle pressure drop is greater than that for its RP-1 counterpart, and causes the fuel pump to operate at a lower flow coefficient near the stall region. Without external control, there is no way known to avoid this occurrence. Adequate component description and component analysis are required for design of a control to avoid problems such as pump stall.

Because of the toroidal configuration, priming of the propellant manifolds is of major interest. The problems in development of main-propellant manifolds for the toroidal configuration are similar to those for conventional bells, but differ in degree for some areas. Two-phase flow dynamics problems at the start are common to both configurations. The analytical and test program will provide data on steady-state and transient fluid flow phenomena such as (1) manifold and injector priming characteristics and repeatability, (2) system pressure drops, (3) manifold volume influence on system

response during throttling and mixture ratio excursions, (4) waterhammer effects or changes of flowrate dictated by start, throttling, or mixture ratio variation, and (5) thrust chamber orientation (vertical and horizontal).

A full-scale transparent model of the LOX manifold has been built, and tests are so scheduled to provide information for design revisions to the breadboard chamber. The tapoff manifold and igniter manifold will be tested for the first time with the breadboard chamber. Although design changes in these systems are not anticipated, they could be made in the full-size hardware after initial tests.

Tests have been made with the LOX manifold installed in both the vertical and horizontal attitude to determine priming characteristics and repeatability, system pressure drops, system response to simulated throttling and mixture ratio excursions, and waterhammer effects. The experimental program was done by photographing (during priming) the jet streams from orifices that simulate the injector around the periphery of the manifold. Time needed between prime of the first and last jets, as determined by analysis of individual frames from the Fastex camera pictures, will be correlated with the data from high-frequency-response pressure measurements for verification of the priming characteristics. It has been determined that (1) uniform priming can be achieved (in less than 30 milliseconds), (2) two tangential inlets function nearly as well as four tangential inlets, (3) radial inlets are probably not desirable, (4) a restriction in one line (as much as 50%) or unequal line lengths cause small effects, (5) centrifugal force separates liquid and vapor during initial priming (this is desirable), (6) torque values are in a tolerable range, and (7) horizontal or vertical position has little effect if inlet pressures are greater than 0.69×10^6 N/m^2 (100 psi).

Two types of full-size toroidal aerospike thrust chambers will be built and tested: a solid-wall workhorse chamber; and two, tube-wall chambers. The relatively inexpensive and rugged, solid-wall workhorse chamber is for early determination of the integrity of the injector and test equipment and igniter testing, all of which would be a moderate risk of damage to the tube-wall chamber. The injector, thrust mount, and structural throat support are identical for both the solid-wall workhorse chamber and the tubular chambers. The breadboard tube-wall chamber is compromised from its flight-weight design to favor hot-firing tests. The structure behind the tubes is heavyweight.

ADVANCED LAUNCH VEHICLES

In spite of the fact that the requirement for a new launch vehicle larger than present ones is not urgent, a limited effort consisting of two major and one minor concepts is being considered. One concept is the plug multi chamber, a cluster of modular bell engines mounted on the periphery of the vehicle's base and surrounding a truncated plug (Fig. 12).
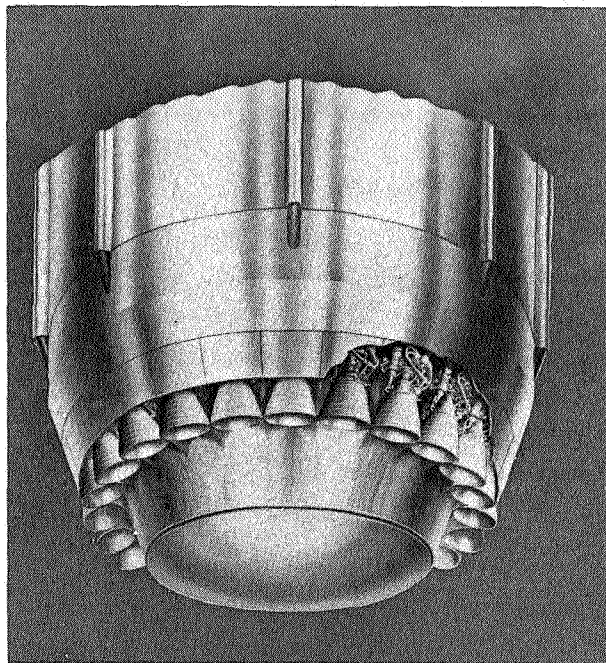

FIGURE 12. PLUG MULTICHAMBER CONCEPT

Another concept is a toroidal chamber around the periphery of the vehicle's base and exhausting onto a truncated plug (aerodynamic spike) in the center (Fig. 13). The other possibility is a group of modular toroidal engines clustered in the conventional manner (Fig. 14).

Analytical studies of the plug multi-chamber concept were made to learn optimum conditions such as the size of the module, the proximity of the adjacent bell chambers, the effect of primary expansion ratio, ways to gain side force, and the effect of plug length.

An experimental program [6] is underway to correlate the data obtained in cold flow testing with those from hot-flow testing. The hot-firing model consists of 18 small rocket engines at 890 N thrust (200 lb thrust) each around a truncated plug (Fig. 15). The individual modules (burning liquid oxygen
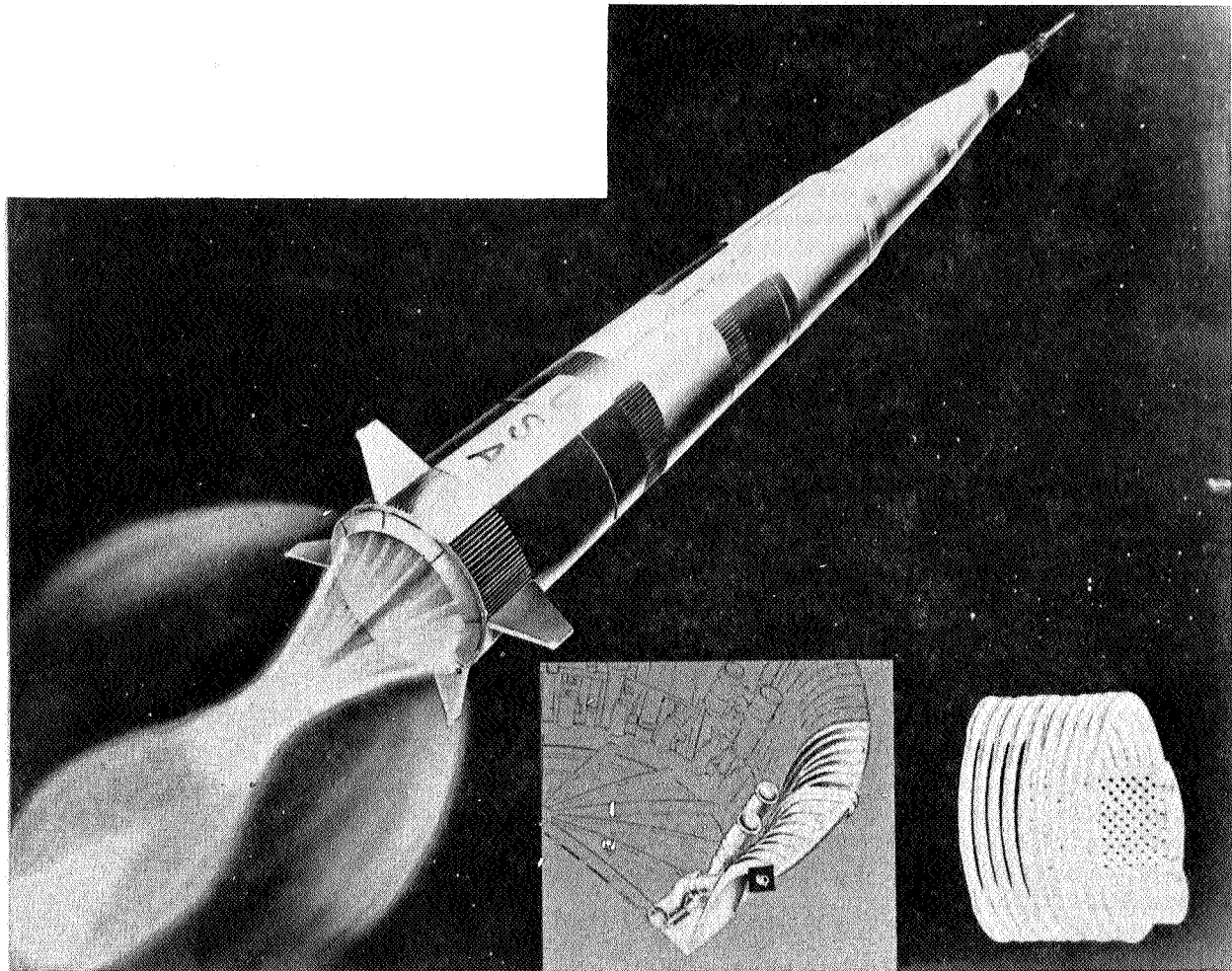
FIGURE 13. TOROIDAL ENGINE APPLICATION

FIGURE 14. CLUSTERED TOROIDAL CHAMBERS

and gaseous hydrogen propellants) are pressure fed from fuel and oxidizer manifolds. The chambers are cooled with high-pressure water. Ignition is by introduction of triethylborane, which is pyrophoric with the oxidizer. There have been some difficulties in igniting the cluster; yet a total of 32 successful tests have been done, with excellent correlation of earlier cold-flow and the hot-flow tests.
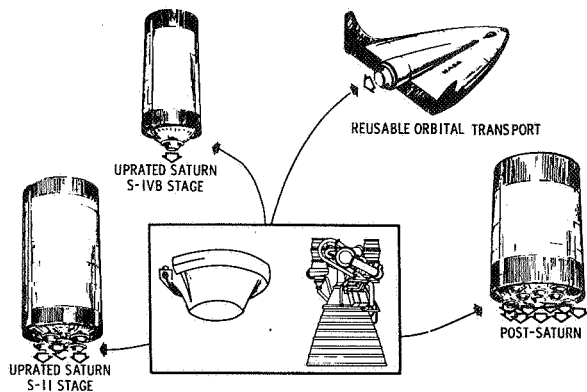
Analytical studies were made of the toroidal concept for large boosters [7], as well as a moderate experimental effort [8]. The purpose was to investigate the feasibility of the toroidal hoop combustion chamber for boosters ranging in diameter from 12.2 to 27.4 m (40 to 90 ft), and in thrust from 80 to 134 MN (18 to 30 M lb). The ultimate objective is data from single-tube and multi-tube segment testing applicable to: (1) evaluation of toroid-nozzle attachment criteria and performance, (2) evaluation of inherent and dynamic stability
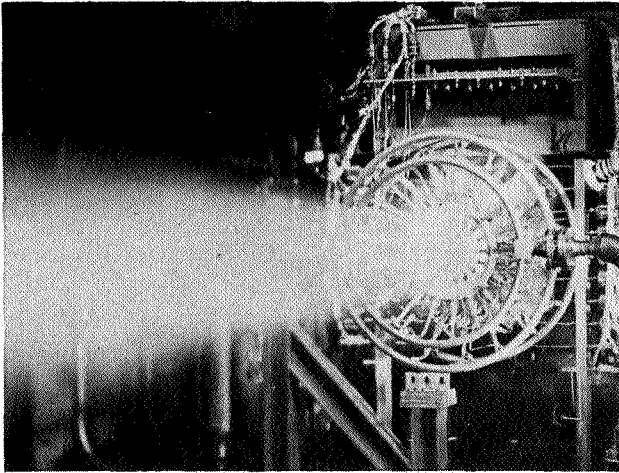
FIGURE 15. HOT-FIRING MODEL OF PLUG
MULTICHAMBER CONFIGURATION

characteristics, (3) evaluation of injector design and tube cooling interactions, (4) evaluation of aerodynamically-shaped sonic tubes, and (5) evaluation of performance losses caused by film cooling and subsequent performance recovery in the nozzle resulting from burning of film coolant.

All data will be applicable to the toroidal concept feasibility for engine systems of advanced future booster configurations.

REFERENCES

1. Advanced Engine Design Study (Bell). Pratt & Whitney, Contract NAS8-11427.

2. Design, Fabricate and Test High Pressure LH_2 Pump. Pratt & Whitney, Contract NAS8-11714.

3. High Pressure LOX Pump. Pratt & Whitney, Contract NAS8-20540.

4. Advanced Engine Design Study (Aerospike). Rocketdyne, Contract NAS8-20349.

5. System and Dynamics Investigation (Special Modification of J-2 Engine Development Contract). Rocketdyne, Contract NAS8-19.

6. Experimental Evaluation of the Plug Multichamber Concept. Pratt & Whitney, Contract NAS8-11438.

7. Toroidal System Analysis. Rocketdyne, Contract NAS8-11402.

8. Feasibility Investigation of the Toroidal Chamber. Rocketdyne, Contract NAS8-4013, and NAS8-21038.

J-2 EXPERIMENTAL ENGINEERING PROGRAM (J-2X)

By

James R. Thompson, Jr.

SUMMARY

Recent experimental work sponsored by Marshall Space Flight Center (MSFC) in the area of large LOX/H₂ engines of the J-2 class is summarized. The work reported is divided into near-term and long range product improvement potential for the J-2 engine. No particular mission applications are emphasized, rather discussion is directed toward operating concepts that allow considerable propulsion simplification of today's system, yet still provide new propulsion capabilities for future Saturn V mission growth. The discussions in this paper are necessarily brief; additional information can be obtained from the author or Messrs. R. A. Byron or D. H. Huang of Rocketdyne, North American Aviation, who have been instrumental in assuring a successful engine program.

INTRODUCTION

Engine programs for the Saturn Launch Vehicle historically have been committed to tight development schedules. The engine configurations, specification requirements and design criteria were limited to those concepts proven satisfactory in the past and which were capable of rapid development. An experimental engine effort was desirable to explore new concepts and ideas and bridge the gap between technology and development. Thus an experimental engineering program was established to assure that advances in current technology are considered and experimentally tested for application to the J-2 engine propulsion system as product improvements. In the specific case of the J-2X program, by taking advantage of the J-2 components and experience, a means is available for evaluation of new concepts while leaving the main J-2 engine development and flight support effort relatively undisturbed. In conjunction with mission needs, a low-cost meaningful decision point is thus provided to determine whether a promising concept should be incorporated into a full-scale development program.

For the past several years the Propulsion and Vehicle Engineering Laboratory at Marshall Space Flight Center (MSFC) has directed the J-2 Experimental Engineering Program as a part of the Manned Space Flight (MSF) supporting development effort. The primary goal of the experimental program was the investigation of new and unique concepts which would improve the performance and operational capabilities of the J-2 engine, with the companion goals of reducing engine complexity, improving launch window flexibility and mission capability, reducing servicing costs, and improving the reliability of the over-all engine related propulsion subsystems. During 1966, a number of these experimental concepts advanced to the extent that they could be seriously considered for further development and incorporation into the Saturn Launch Vehicle. These concepts are briefly discussed in the following paragraphs along with their more significant potential contributions to the launch vehicle.

The experimental engine does not have a fixed description or drawing specification, but is rather a test article which constantly changes configuration. The experimental engine basically resembles the J-2 engine, burns liquid hydrogen and liquid oxygen, and is rated at 1.02 MN (230 000 lb) thrust in vacuum. The basic configuration consists of a regeneratively cooled 27.5:1 expansion ratio thrust chamber which has been modified at the forward end to incorporate a hot-gas tapoff system for turbine drive, a liquid hydrogen and a liquid oxygen turbopump with turbines connected in series and driven by hot gases extracted directly from the thrust chamber combustion zone, main and auxiliary valves and sequencing control logic. Thrust and propellant mixture ratio control is obtained by varying the control orifices in the hot gas turbine drive system.

NEAR-TERM SATURN PROPULSION IMPROVEMENTS

Emphasis during the early part of the past year was directed toward establishing a total engine system that would be capable of reliable operation without the extensive thermal conditioning of the engine and propellant feed system hardware prior to an engine firing. As shown in Figure 1, using the
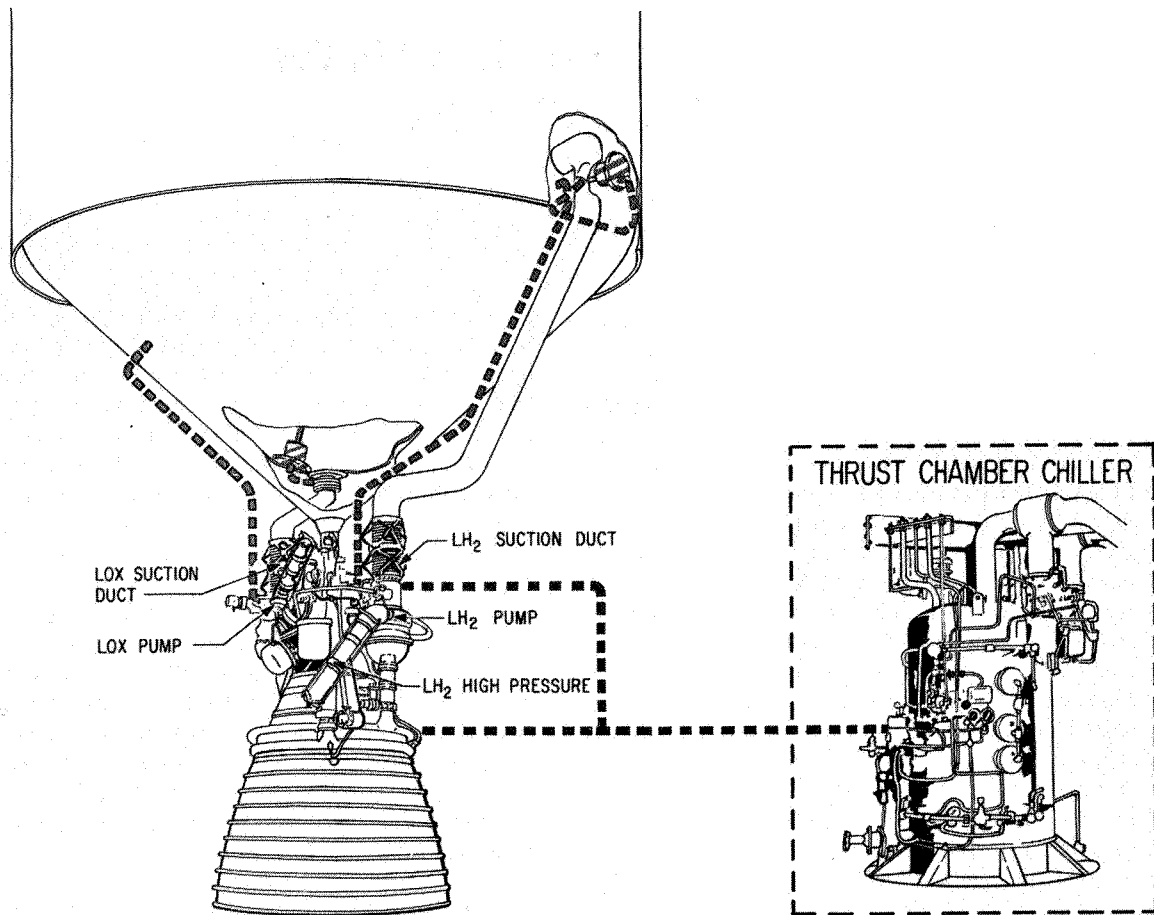
FIGURE 1.   J-2 ENGINE PRECONDITIONING FOR START

J-2 engine/S-IVB stage propulsion unit as an example, there are four major areas in today's propulsion system which require hardware conditioning with associated complex operational procedures, costly checkout, and cumbersome ground support equipment (GSE). Briefly, the current propulsion configuration requires both hydrogen and oxygen propellant circulation through the engine/stage feed ducting and engine turbomachinery to assure having adequate liquid propellants and ample net positive suction pressure at initiation of engine start. This is accomplished with small electric driven pumps mounted near the bottom of each propellant tank in ducting joining the main propellant feed lines. Propellants are returned to the stage via separate ducting indicated by heavy dashed lines in the figure. Other areas requiring thermal conditioning are (1) the engine mounted hydrogen bottle used in storing gaseous hydrogen that provides initial starting energy to the engine turbines, and (2) the regenerative thrust chamber tube bundle which must be chilled below 200°K (-100° F) to remove the sensible heat and reduce the

hydraulic resistance in the hydrogen flow passages. Both of these subsystems are serviced by ground equipment as indicated in Figure 1. The S-II Stage propulsion system is quite similar, although natural convection of the oxygen through the circulation ducting is used rather than forced pumping.

Eliminating only some of the above described procedures or relaxing operational red line values was not considered as an acceptable program goal, and the experimental effort on the engine was directed toward defining and applying test discipline to a configuration that would completely eliminate all of the above conditioning requirements. To accomplish this, the engine cycle was changed from one employing a gas generator to provide turbine power, to one tapping off combustion gases at approximately 922°K (1200° F) from the thrust chamber to drive the series turbines. Figure 2 provides a cut-away view of the hot-gas tapoff area immediately downstream of the injector face. Early testing indicated that obtaining a consistent tapoff gas temperature would not be a major problem as first
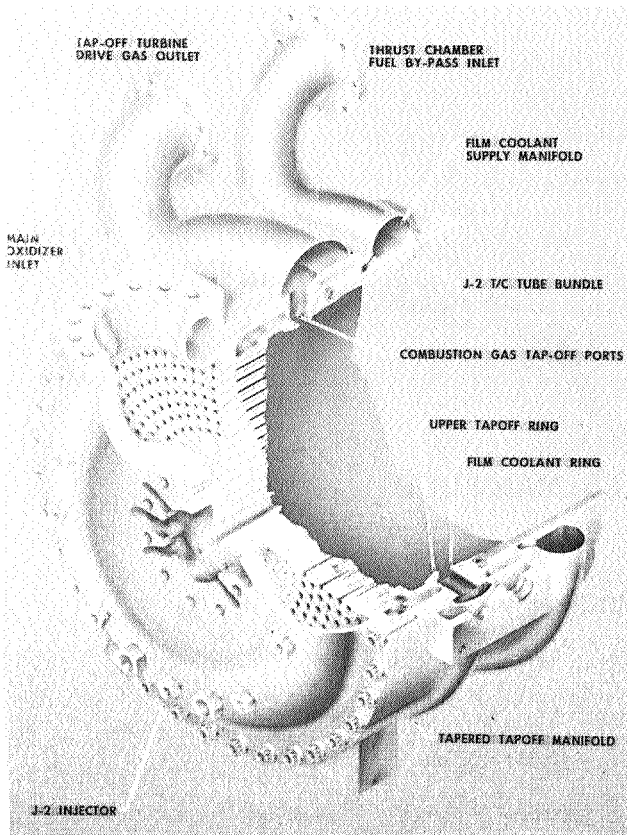
FIGURE 2. J-2X TAPOFF SYSTEM

imagined, but that considerable design effort would
be required to obtain a configuration that would
provide proper hardware cooling in the immediate
tapoff area. The hardware erosion problem pri-
marily centered around the area immediately down-
stream of the tapoff section illustrated in Figure 3
because the oxidizer was not making the rapid turn
to the tapoff manifold as easily as the lighter hydrogen
and was thus striking the chamber wall. To date the
solution appears to be in film cooling this area with
hydrogen supplied by a separate manifold shown in
the lower right hand area of the cross-section. Thus
far in the program over 300 engine tests on eleven
separate configurations have been evaluated using
this concept for turbine drive. Over 4000 sec of
mainstage operation have been logged with the
longest single test lasting 200 sec (the duration
limit of the experimental test facility).

Considerable experimental testing has been di-
rected toward integrating the tapoff gas cycle concept
into an operational engine starting sequence to achieve
the desired simplification. A schematic of the total
engine cycle is shown in Figure 4 accompanied by
the following description of some of the more unique

features. To accomplish propellant and engine
hardware conditioning and at the same time provide
a settling force to propellant tanks, the engine
operates in a low-thrust mode of operation termed
"idle mode." During idle mode, the turbomachinery
is not rotating and propellants are driven by tank
pressures only. The duration of idle mode would be
mission dependent to account for the propellant and
hardware conditions prior to its initiation. As an
example, the duration of idle mode for restart of
the S-IVB Stage in the Saturn V LOR mission is
estimated to be 50 sec. During this mode of operation,
the engine would be capable of producing low impulse
bits at thrust levels of approximately 26 700 N (6000
lbs) for additional applications such as stage deor-
biting, orbit transfer, staging, gross docking
rendevous, attitude control, and other pulse-mode
duty cycles. The idle mode engine operating cycle
is shown in Figure 5. At this time, it appears
maximum idle mode duration should only be limited
by the propellant supply. The engine cutoff sequence
is designed for a mainstage to idle mode transition;
the idle mode thrust provides for propellant slosh
control in the vehicle prior to complete shutdown.
Three solid-propellant turbine starters (SPTS)
mounted on the fuel turbine manifold provide triple-
start capability for the S-IVB Stage. The solid
propellant turbine start eliminates the need for a
gaseous hydrogen start tank with its cumbersome
procedures and GSE, and provides the necessary
initial turbomachinery power to flush the mixed-
phase propellants from the feed ducting and engine
during the starting transition to mainstage operation.
The burn time of the solid propellant motors is
approximately 2 sec in duration and is tailored to
provide a gradual but positive buildup in pump speed
assuring (1) ample stall margin of the fuel pump,
and (2) a consistent starting transition resulting
from the relative insensitivity of the solid propellants
to the harsh duty cycle environment of the J-2 engine.
The requirement to thermally condition the thrust
chamber can be eliminated by bypassing most of the
hydrogen around the thrust chamber during the
starting transient operation and feeding the fuel
directly into the injector and tapoff coolant manifolds.
During the past year, this technique of simplifying
the engine operation has been demonstrated as
technically sound and with proper development will
provide reliable engine starting with chambers
initially at room temperature or warmer. The
mechanism which prevents the current engine from
ambient chamber starting is the rapid buildup in fuel
pump back pressure created by the hydraulic resist-
ance in the regenerative tube bundle. Excessive
back pressure will stall the fuel pump. This is
alleviated with the bypass feature which unloads the
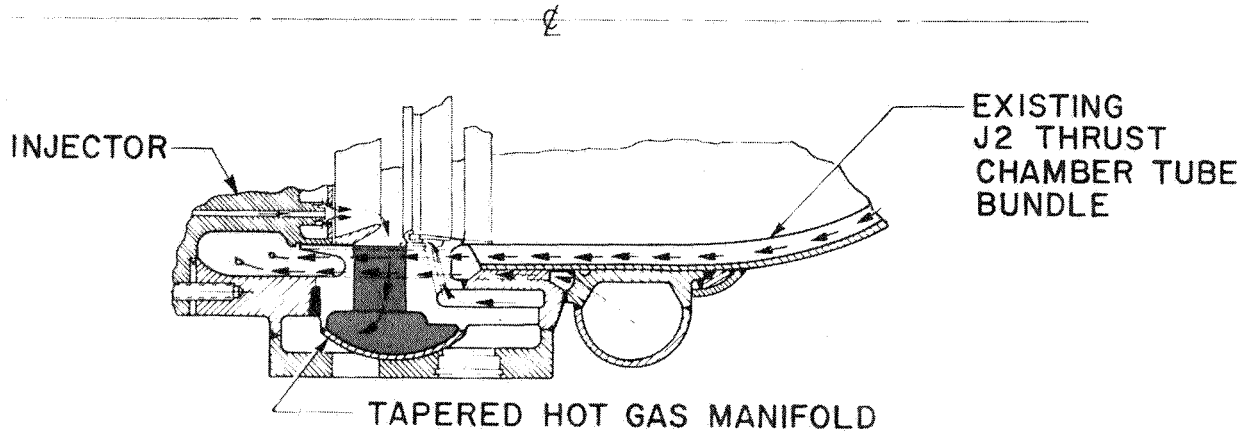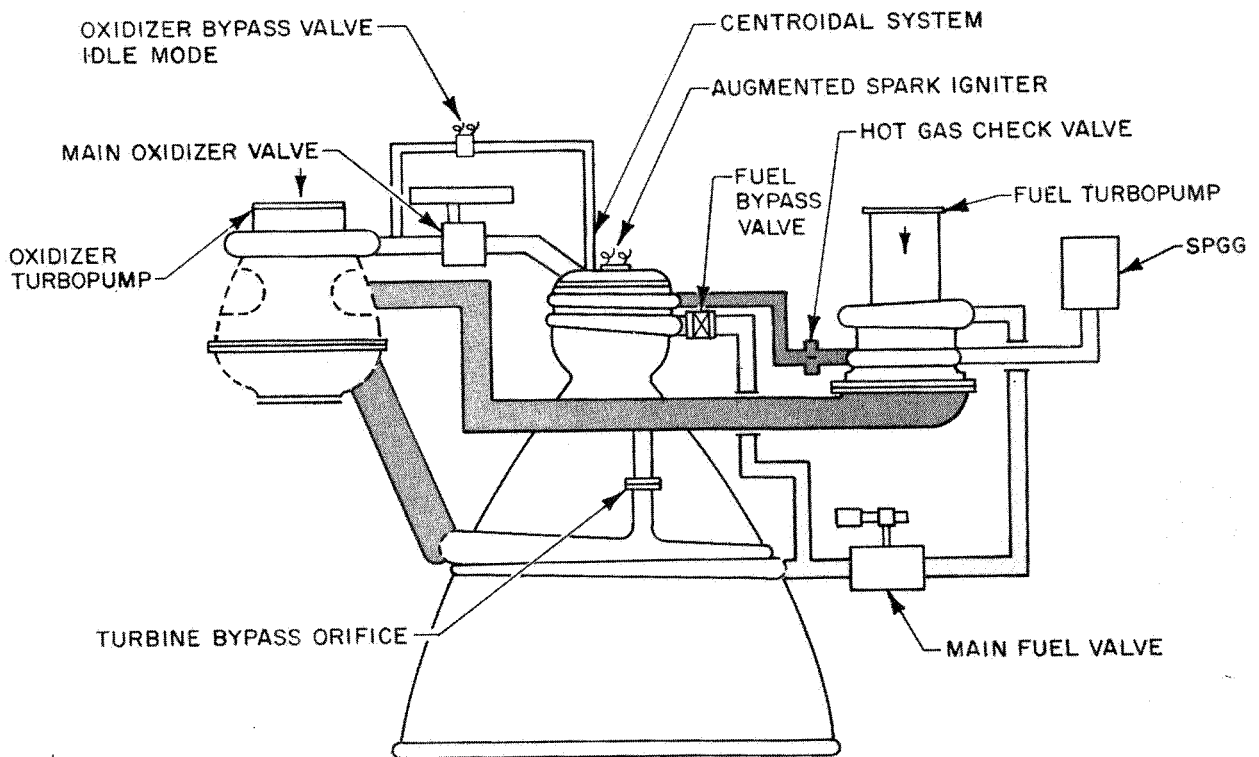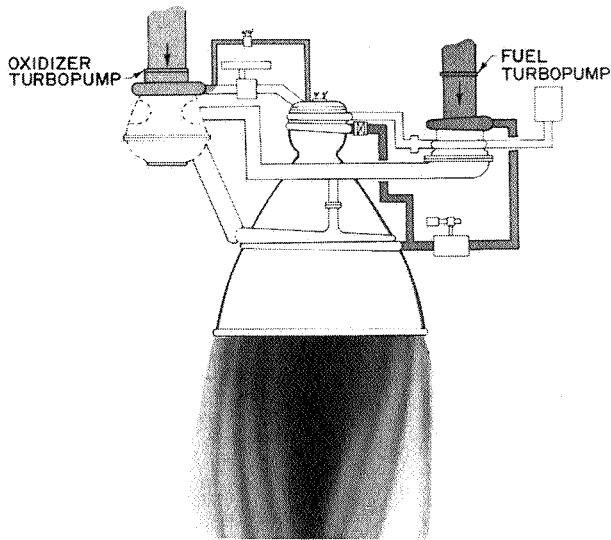
FIGURE 3. J-2X TAPOFF AREA

FIGURE 4. SYSTEM OPERATING CONCEPT

pump pressure during the critical early portion of the transient operation. Once propellant flow is well established and the chamber is cooled by hydrogen in the regenerative tubes, the bypass system is

- PROPELLANT ULLAGING

- DEORBITING

- GROSS RENDEZVOUS
  FOR DOCKING

- PLANE CHANGES

FIGURE 5.   EXPLOITING IDLE MODE
OPERATION

closed and all the hydrogen is routed through the chamber for mainstage cooling. Thus, another set of pre-start conditioning procedures can be eliminated by functionally accomplishing the same job within the normal sequence of engine starting events.

The significance to the Saturn Launch Vehicle of the engine operational simplification discussed in the preceeding paragraphs can readily be assessed by a comparison of the terminal launch sequence of events that were required on flight AS-201, illustrated in Figure 6, as opposed to that which would have been required with the propulsion system simplifications described above and illustrated in Figure 7. The pre-launch events for the S-II Stage can be reduced by a comparable amount for each engine. In addition to a reduction in operational procedures, considerable hardware and servicing subsystems can be removed from the stages by reducing these engine conditioning requirements as seen in viewing the S-II Stage engine compartment area "before" and "after" illustrations shown in Figure 8.

A considerable number of events associated with thermally conditioning the engine, the propellant feed ducts, and settling the propellants, occur after vehicle launch and can be further reduced by implementing the system concepts discussed above. Figures 9 and 10 graphically identify these events by name and relate them to time after liftoff.
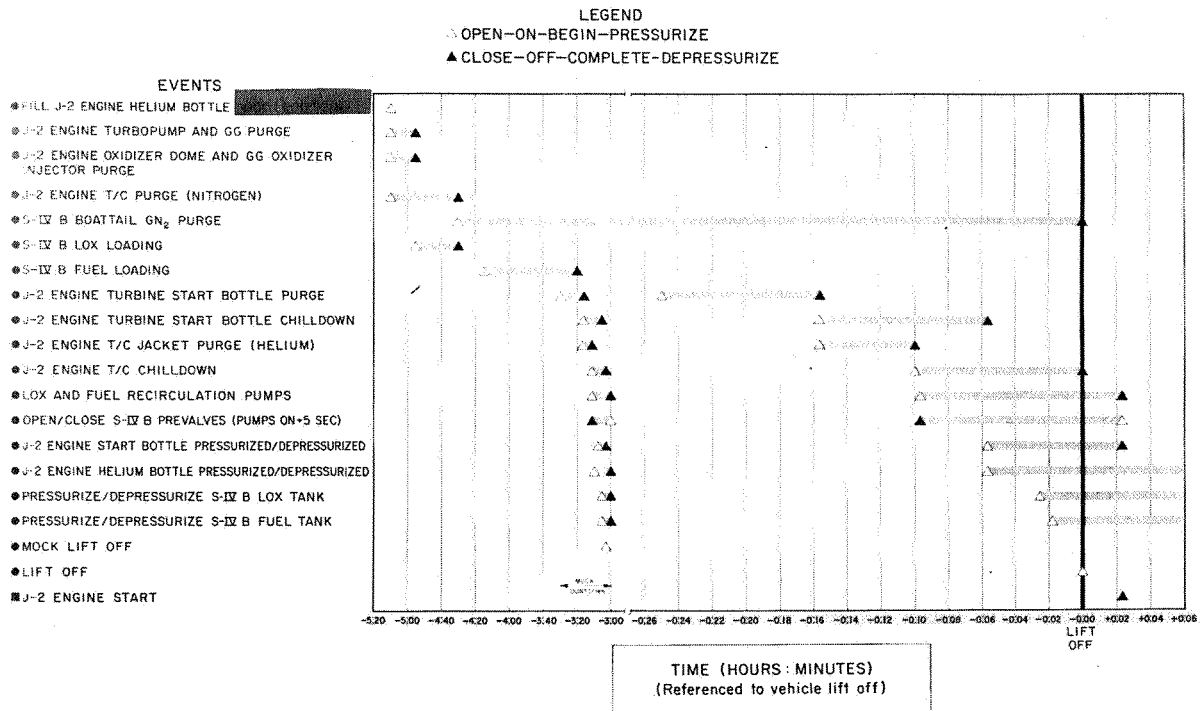

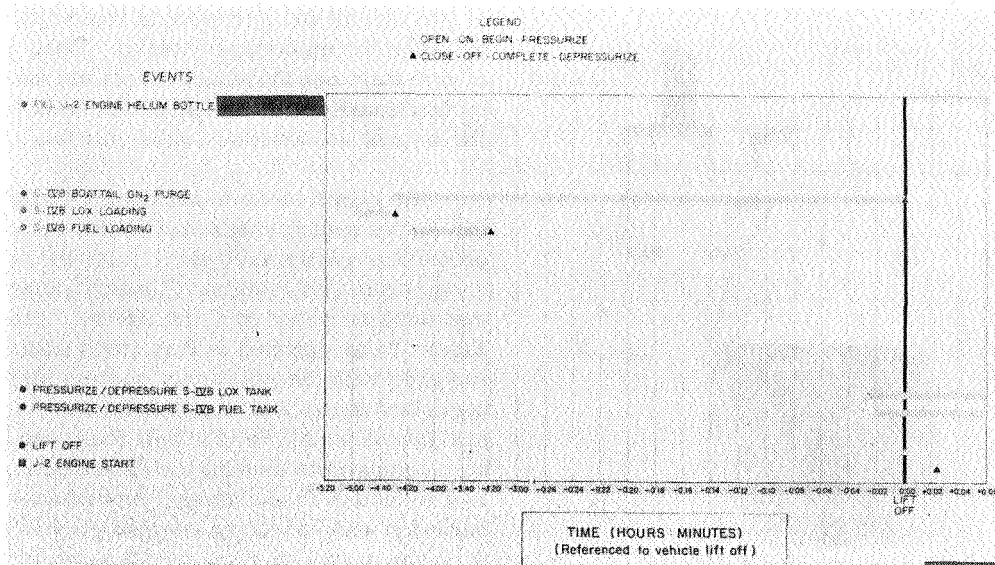FIGURE 6.   FLIGHT 201 S-IVB STAGE PRE-LAUNCH CONDITIONING EVENTS

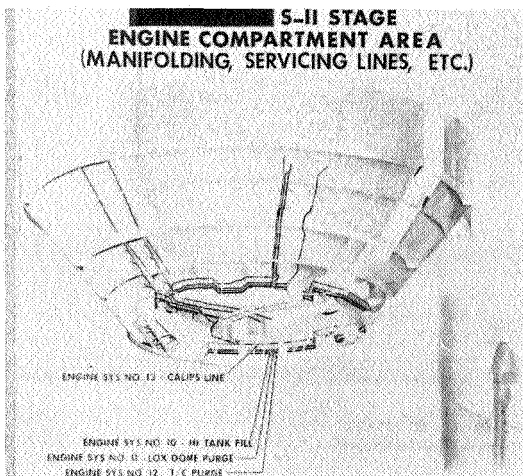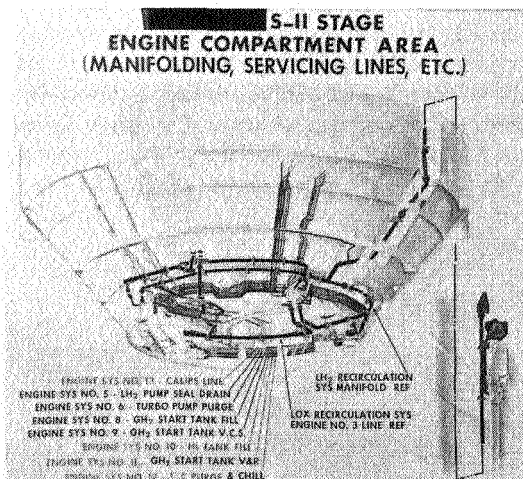FIGURE 7. POTENTIAL S-IVB STAGE PRE-LAUNCH CONDITIONING EVENTS

FIGURE 8. S-II STAGE ENGINE
COMPARTMENT AREA

During the time that the J-2X program has been under contract with Rocketdyne, MSFC propulsion personnel have continually assessed the impact on the Saturn Launch Vehicle of incorporating into the Saturn Program those specific engine features which have promise of being technically sound. More recently these analyses, in conjunction with the Douglas Aircraft Co. and Space & Information Systems Division of NAA, have concentrated on a detailed investigation of the propulsion features described earlier. In addition to an overall reduction in static firing and launch pre-test procedures and operational simplifications, the S-II Stage analysis has indicated the following elements can be deleted from the stage recirculation and pressurization systems:

1. 176 m (576 ft) of engine and pressurization system manifolds.

2. 26.2 m (86 ft) of vacuum jacketed lines.

3. several batteries.

4. five hydrogen recirculation pumps, motors and inverters.

5. eleven LOX and LH_2 shutoff valves.

6. seven umbilical connections.

7. 79 tubing joints.

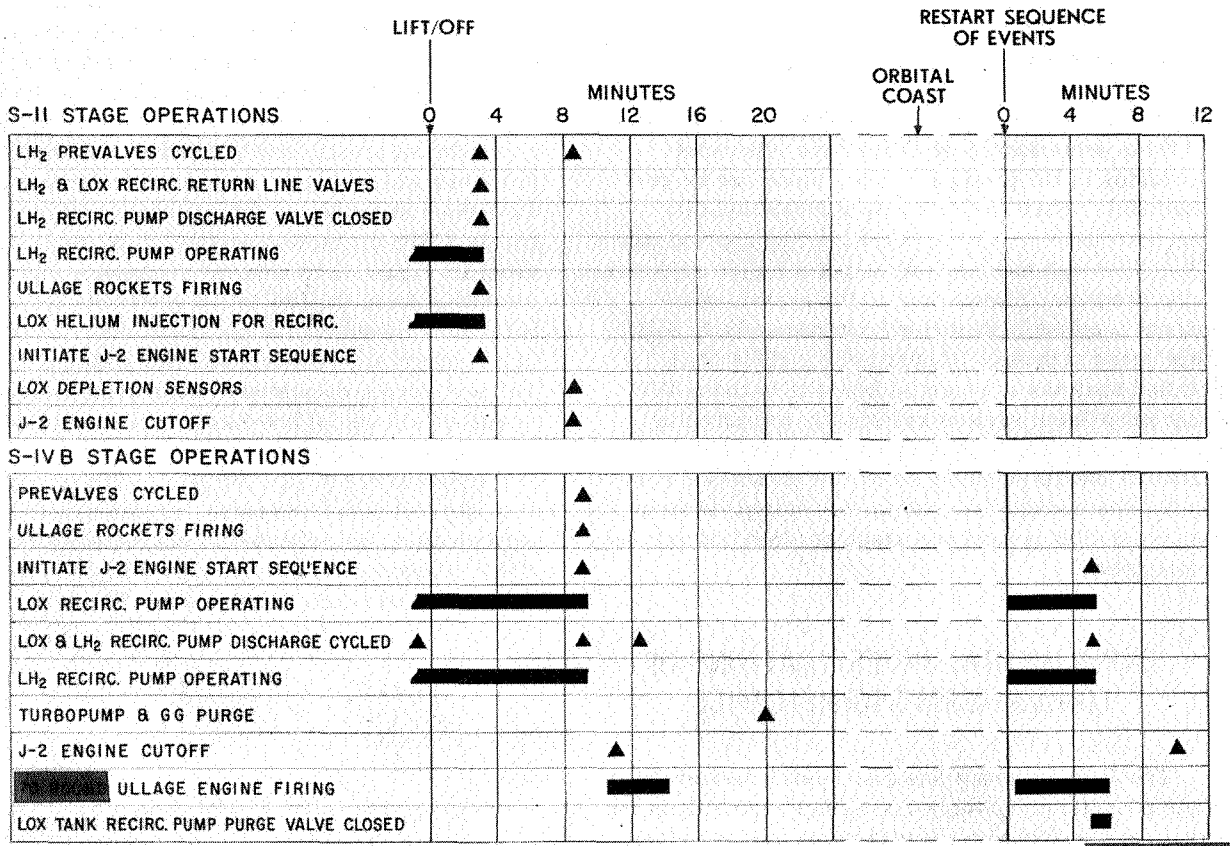8. 58 seals.

9. three helium bottles.

FIGURE 9.   CURRENT SATURN V INFLIGHT PROPULSION OPERATIONS (J-2 ENGINE REQUIREMENTS EXCLUDING TANK PRESSURIZATION)
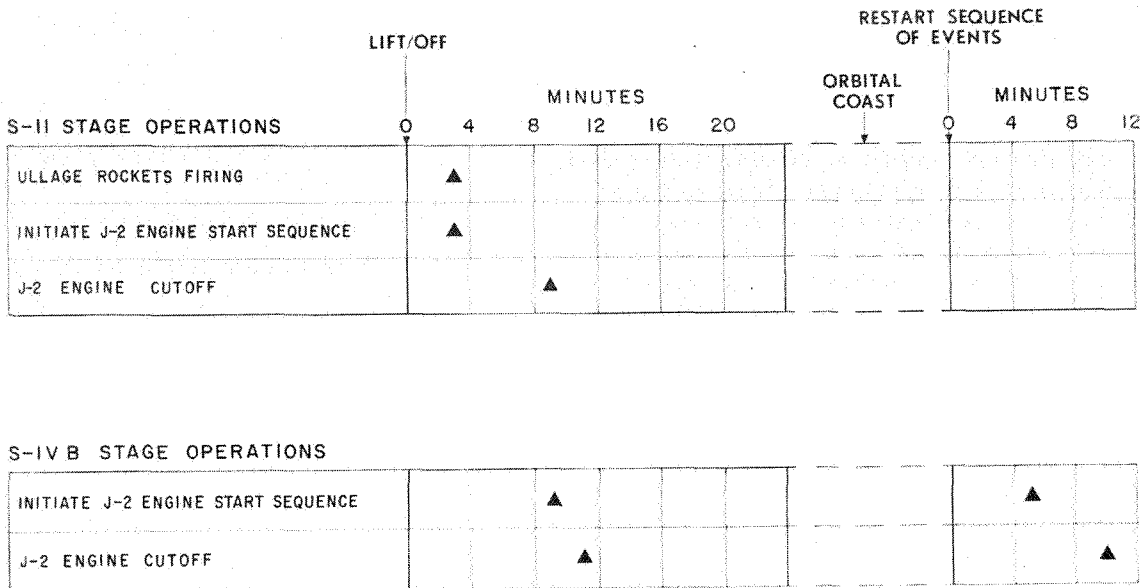

FIGURE 10.   POTENTIAL SATURN V INFLIGHT PROPULSION OPERATIONS (J-2 ENGINE REQUIREMENTS EXCLUDING TANK PRESSURIZATION)

10. five check valves.

11. 18 flexible hoses.

Accruing from the elimination of this hardware and from procedural simplifications, checkout operations in the propulsion area alone can be reduced 36%. Study results also indicate existing stage unreliability can be decreased by approximately 30%. Although mass saving is not a major objective of the program, elimination of the system components previously described can result in a S-II Stage mass reduction of over 908 kg (2000 lbs). A detailed analysis of potential benefits to the S-IVB Stage propulsion system are equally encouraging. Current plans are to further demonstrate the technical merits of this type of J-2 propulsion system by functionally integrating a prototype system with the S-IVB ground test stage at MSFC during the coming year.

EXPERIMENTAL INVESTIGATIONS OF LONGER-TERM SIGNIFICANCE

The J-2X program has also been investigating other propulsion concepts that to date are still in the early phases of experimental testing. Some of the initial results are particularly significant and fall into three areas of experimentation: (1) controlled deep throttling, (2) minimizing starting transition chamber side loads, and (3) tank head starting for multi-restarts.

These results should provide technology for any advanced or uprated LOX/H$_2$ engine configuration as well as for later versions of the J-2 class. To experimentally evaluate these features, J-2X engine 011 was built to incorporate all of the engine characteristics and capabilities previously described, in addition to (1) a thrust chamber truncated at an area ratio of 16.5:1 to evaluate chamber side loading at full and reduced thrust levels at sea level, (2) turbopump clearances modified to reduce required break-away starting torques to enhance tank head starting, (3) a recycle system around the hydrogen pump to provide added pump stall margin at reduced thrust levels, and (4) additional control valves for system throttling. These four engine features are discussed in detail in the following description of test objectives and results. Thirty-five firings for an accumulative test time of 634 sec were conducted on the J-2X 011 engine system.

Engine System Throttling. The specific objectives of the throttling program were to (1) evaluate

engine performance at the lower thrust levels with respect to chamber combustion efficiencies and the combustion and system stability characteristics, (2) establish the system gains and engine control requirements to achieve steady state operation at the lower thrust levels, and (3) define chamber heating problems which may be encounted under sea level conditions at the lower thrust levels with a separated nozzle. The ultimate objective of the throttling program would be to achieve continuous and stable transition from the low thrust pressure-fed idle mode to turbine driven engine operation over the entire thrust range at a constant mixture ratio of 5.0:1. The test series consisted of eight tests, accumulating a total of 450 sec of hot-firing with the engine being throttled from mainstage chamber pressure levels of approximately 4.82×10^6 N/m^2 (700 psia) to a low of 0.55×10^6 N/m^2 (80 psia), or near 10:1. Chamber performance, as reflected in characteristic velocity (C*) efficiency, remained high over the throttle range as graphically illustrated in Figure 11. High
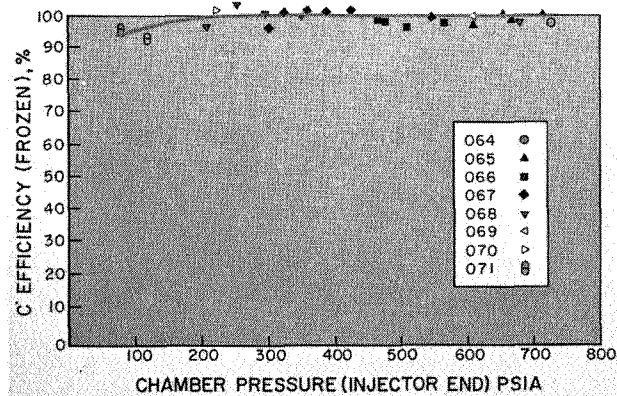
J-2X Throttling Result Summary:

1. Eight tests were conducted for total of 450 sec.

2. Stable engine operation was achieved at a chamber pressure of 0.55 MN/m^2 (80 psia) and engine mixture ratio of 2.37.

3. Combustion instability was encountered during one test.

4. Chamber C* efficiency remained high throughout throttling range.

FIGURE 11. C* EFFICIENCY VS CHAMBER PRESSURE

frequency combustion instability occurred on one test and was analyzed as resulting from a combination of low chamber mixture ratio (hydrogen injection temperatures were near those of liquid hydrogen temperatures) and several tube splits in the regeneratively cooled combustion zone. During this series of engine tests, low frequency or chugging instability in the combustion chamber has never occurred, nor was there any evidence of instability in the hydrogen drive system between the pump and the thrust chamber tube bundle. Control of chamber pressure and mixture ratio was adequate from main-stage chamber pressure levels of 4.82×10^6 N/m^2 (700 psia) to approximately 1.38×10^6 N/m^2 (200 psia). At pressures lower than 1.38×10^6 N/m^2 (200 psia), the experimental control system could not maintain a near constant mixture ratio, resulting in the chamber mixture ratio drifting to about 2.0:1 at the 10% thrust level and thereby considerably reducing the hydrogen injection temperature. With the exception of the combustion instability at the off-design mixture ratio, no problems were encountered over the entire throttle range. The control points used in the engine system to achieve throttling were (1) a control valve in the hot-gas tapoff duct between the chamber and fuel turbine, (2) a control point bypassing the oxidizer turbine, and (3) a fuel recycle path from the pump discharge to inlet. The fuel recycle path was added to avoid the fuel pump

stalling at the reduced thrust levels by maintaining pump flow at a relatively high value. Conceptually, the system used is shown in Figure 12. During this test series, approximately 0.0316 m^3/s (500 GPM) were recycled around the fuel pump at the 50% thrust level and provided an additional 0.0316 m^3/s (500 GPM) of stall flow margin. No effort was made to define the effect on pump suction performance, which will be evaluated in subsequent testing. The fuel pump head flow map (Fig. 13) graphically illustrates how the engine was throttled and the control points used at each level. The hot-gas tapoff control throttled the system, at a near constant mixture ratio, to approximately the 60% thrust level, at which time the engine mixture ratio was reduced to approximately 4.0 with the oxidizer turbine bypass control. After opening the fuel pump bypass valve to provide added stall margin, the thrust was further reduced to the 10% level by a combination of the tapoff control and the turbine bypass valve as shown. A sketch of the engine system with control points is shown below the pump map. The lines of constant mixture ratio and constant chamber pressure will assist in identifying the control gains on engine performance.

One mission application for an S-IVB Stage using J-2 class engines capable of throttling is illustrated in Figure 14 and shows the stage used as a shelter on
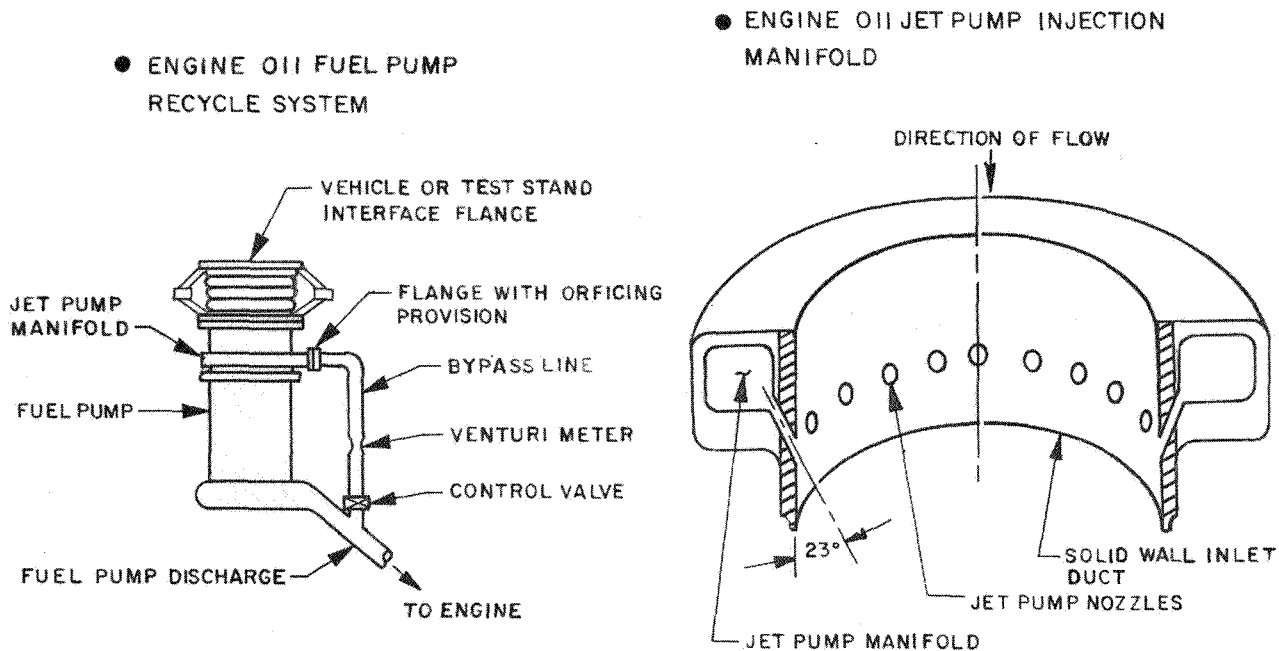

FIGURE 12. J-2X 011 FUEL PUMP RECYCLE SYSTEM
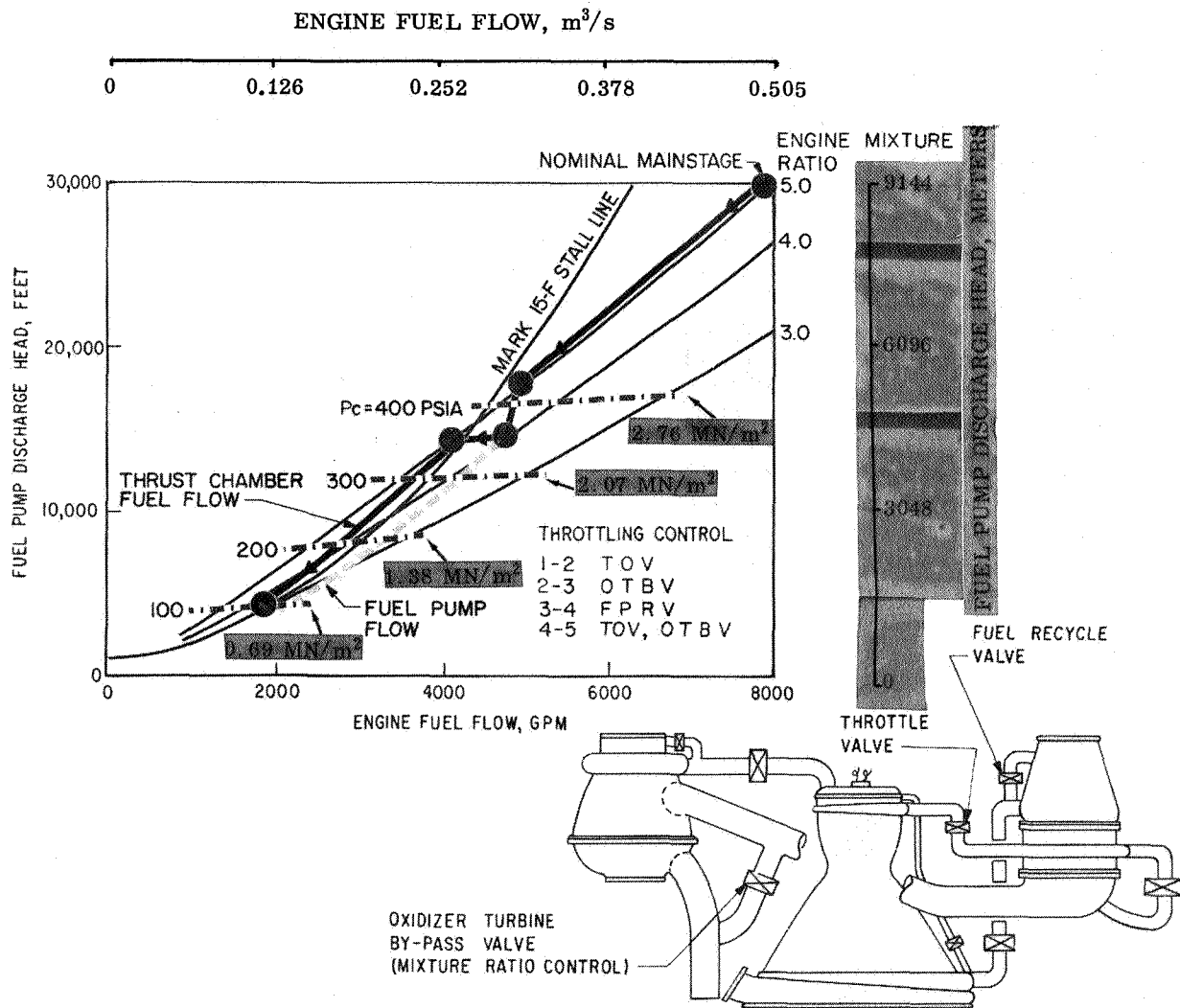
ENGINE FUEL FLOW, m³/s

FIGURE 13.   J-2X ENGINE 011 FUEL TURBOPUMP THROTTLING MAP

the lunar surface. Missions of this type are used to identify typical performance characteristics for experimental analysis (such as throttling rates, levels, etc.) which may be required for possible future development.

During 1967, Rocketdyne will continue to work on additional engine systems to further define engine throttling capability. Early in 1967, a pressure-fed injector/thrust chamber component throttling program is planned at MSFC to provide additional data and assist in establishing the performance and response characteristics of the injector/chamber from 8900 to 890 000 N thrust (2000 to 200 000 lb thrust) over a mixture ratio range of 3 to 6. The facility to be used at MSFC is currently being prepared (Fig. 15)

Chamber Side Load Reduction. Considerable effort has been expended to minimize or eliminate the starting and cutoff transient thrust chamber side loading that currently exists on all J-2 engine firings at sea level conditions. Under sea level conditions during engine development, production acceptance and stage acceptance testing, the thrust chamber is currently restrained during the starting transition to prevent engine damage. Figure 16 illustrates a typical installation when static firing the J-2 engines installed on the S-II Stage. During the past year, studies were conducted to investigate methods of reducing the chamber transition loading to an acceptable level where restraining mechanisms would not be required, yet still meet the requirements of a full flowing nozzle at mainstage operation. Since the present J-2 chamber contour produces a slowly
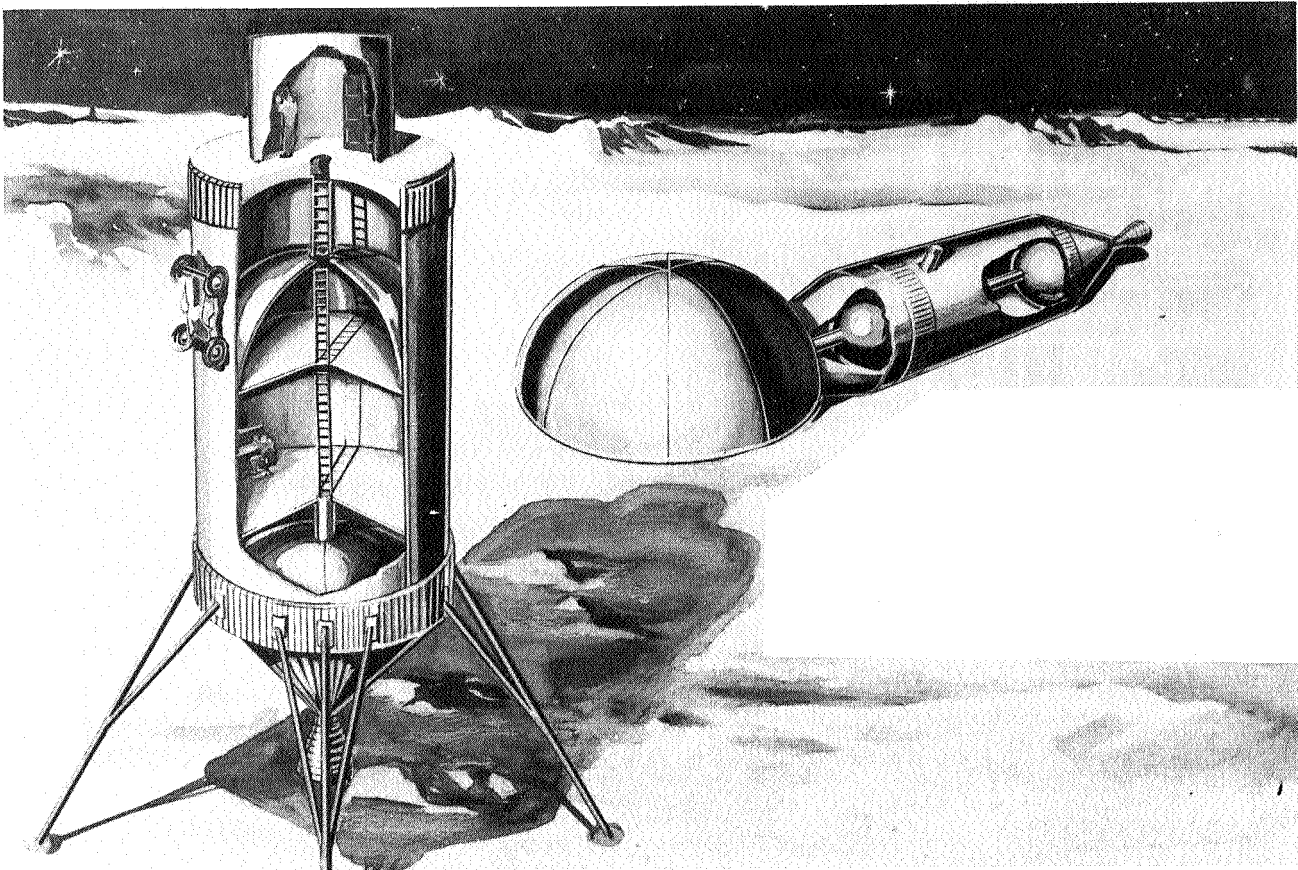
FIGURE 14. S-IVB SPENT STAGE APPLICATION ON LUNAR SURFACE

decreasing pressure profile downstream of the chamber throat and then an increasing pressure gradient from an area ratio of approximately 22:1 to the chamber exit (ϵ = 27. 5:1), this has become the prime suspect causing the excessive transition side loads on the current J-2 nozzle. In comparison to other nozzle contours, an early effort was directed toward evaluating the effect of this type of contour on the side loading during transition. Wind tunnel testing indicated that the side loading could be substantially reduced with steeper pressure profiles continuously decreasing from the throat plane to the nozzle exit. To arrive at a nozzle design for full scale fabrication and testing, a series of wind tunnel tests were run with continuously decreasing pressure profiles at several levels of wall pressure at the nozzle exit, and a compromise design was chosen.

The contour selected has a 37 degree initial divergence angle downstream of the throat and a 3. 5 degree angle at the nozzle exit. The 37/3. 5 nozzle was selected because it had the highest exit wall pressure of those tested for a nozzle with a continuously decreasing pressure profile (to assure having a full flowing nozzle at mainstage operation), yet would still produce nozzle performance characteristics at full thrust that were comparable to those of the current J-2 design.

To obtain some early indication as to the validity of the hypothesis that the side loading can be reduced if the pressure profile continuously decreases from the throat to the exit, the J-2X engine 011 nozzle was truncated at approximately an area ratio of 16. 5:1 and tested. However, during these tests, the turbine
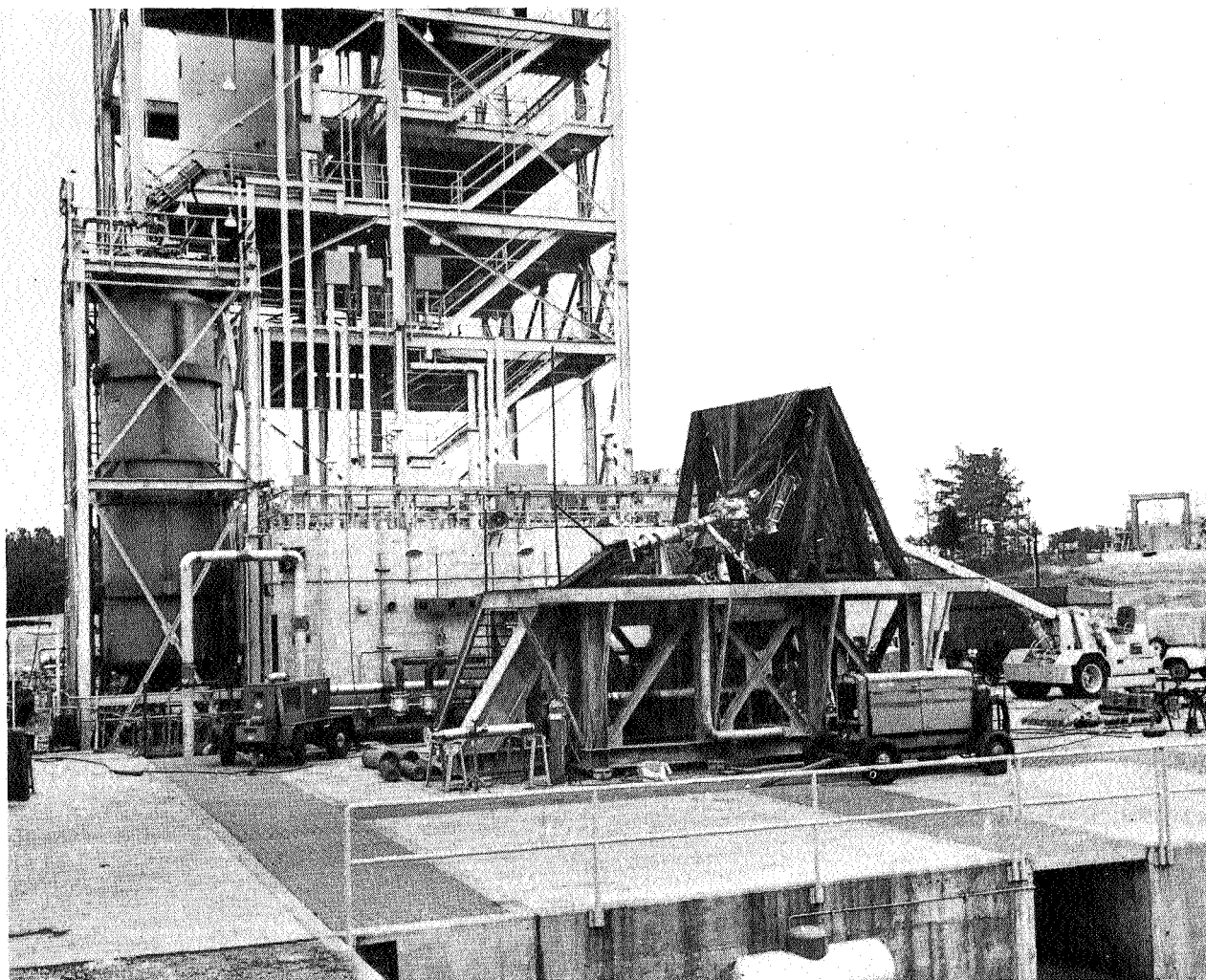
FIGURE 15. MSFC FACILITY FOR PRESSURE-FED THROTTLING TESTING

exhaust gases were ducted overboard rather than being returned to the chamber at an approximate area ratio of 12:1 as is done in the current J-2 design. (There is some opinion that injection of these gases may in some way assist in triggering the transition side loading by inducing asymmetric separation.) The results from engine 011's testing were quite encouraging because both starting and cutoff transition loading were substantially reduced as measured by load cells located in outrigger arms attached to the nozzle. Also of interest during the throttling testing (at sea level) discussed earlier, there were no appreciable loads measured that compared to those of the current J-2 transition loads.

These data are summarized below and graphically illustrated in Figure 17.

1. The thrust chamber side load magnitude and duration were significantly reduced from those received with the 27.5:1 chamber.

   a. Maximum loads during start were reduced from 62 200 N thrust (14 000 lbs thrust) (J-2) to 18 700 N thrust (4200 lbs thrust).

   b. Transient duration during start was reduced from 1.0 sec to 0.5 sec.

   c. Maximum loads during cutoff were reduced from 89 000 N thrust (20 000 lbs thrust) (J-2) to 13 330 N thrust (3000 lbs thrust).

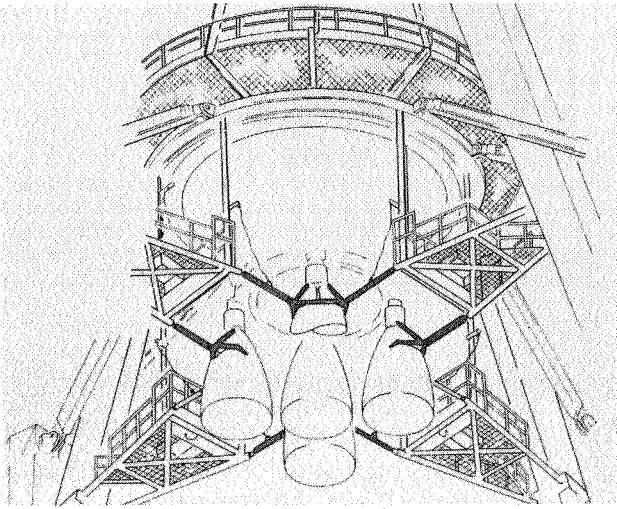   d. Transient duration during cutoff was essentially unchanged.

FIGURE 16. SIDE LOAD ARRESTING MECHANISM (SLAM) FOR STATIC TEST – S-II STAGE

2. The throttling side loads reached a maximum of 8450 N thrust (1900 lbs thrust) at 1.62×10^6 N/m^2 (235 psia) chamber pressure.

Fabrication of a full-scale chamber of the 37/3.5 design is scheduled for completion in early 1967 and will be tested shortly thereafter. Successful results from these tests (i.e., indications that restraining mechanisms are not required when starting at sea level) would provide the information to develop this capability into the J-2 engine should this feature become a Saturn Program requirement.

Tank Head Starting. Although use of the solid propellant turbine starters (SPTS) provides considerable improvement over the current J-2 hydrogen spin bottle in terms of thermal pre-conditioning and servicing, for some of the more advanced missions requiring days in orbit between engine starts, it appears highly desirable to eliminate any need for external initial power to the turbomachinery as provided by the SPTS. This becomes particularly important if the orbital environment at the time engine start is required cannot be predicted, or if the number of starts to mainstage operation prohibits use of the SPTS from strictly a mass standpoint. For these reasons, engine starting by vehicle propellant tank pressures only (tank head starting) has been aggressively pursued in the J-2X Program. Although as of the end of 1966, the number of engine tests (three) conducted without assistance from the SPTS were not impressive, the results from these
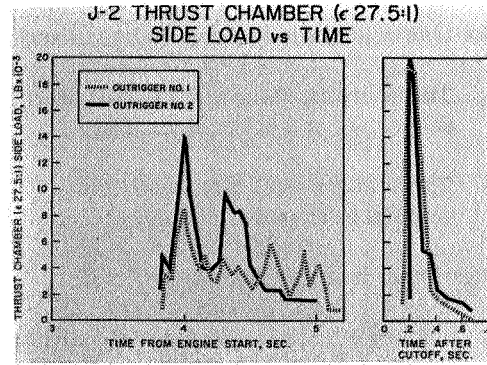
psia						
100	200	300	400	500	600	700
0.69	1.38	2.07	2.76	3.42	4.13	4.82

N/m$^2 \times 10^6$

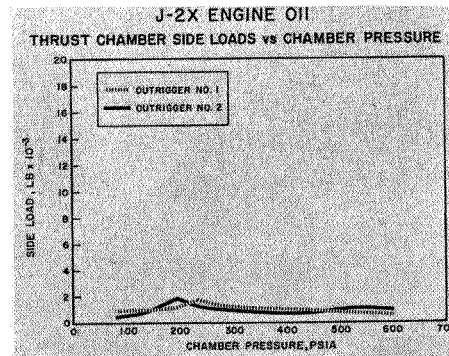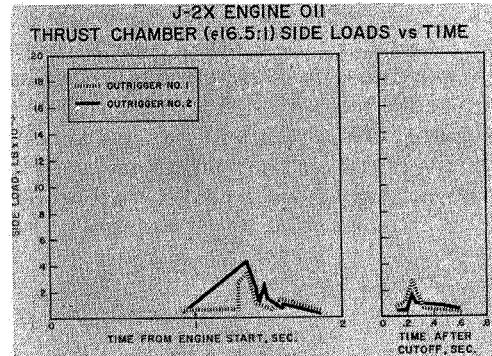| lb thrust $\times 10^{-3}$									
2	4	6	8	10	12	14	16	18	20
0.89	1.78	2.67	3.56	4.45	5.34	6.23	7.12	8.00	8.90

N thrust $\times 10^{-2}$

FIGURE 17. THRUST CHAMBER SIDE LOADS DURING ENGINE STATIC FIRING

tests were encouraging enough to warrant spending considerable effort in this direction in 1967. To date, the following results have been obtained:

49

1. Six tank head start tests were conducted.

   a. Three preliminary tests established sequence control requirements.

   b. Three successful tank head starts were completed to mainstage operation.

2. Significant test results were –

   a. 8.5 sec elapsed from start signal to 90% chamber pressure.

   b. Excellent consistency was obtained.

3. Improved sequence control should result in a starting time of 7.0 sec at sea level.

FIGURE 18.   TANK HEAD START SUMMARY

Figure 18 illustrates the consistency of transient operation evident on the tests attempted. Based on the engine starting concept discussed earlier, in the opinion of the author, several problems can be expected in the development of a tank head start J-2 engine which is common for all applications. Primarily, it is felt that the function the SPTS serves on the S-II Stage and S-IVB Stage (1st burn) of rapidly purging the propellant feed ducts of warm propellant cannot easily be replaced by a tank head start because for these applications the vehicle has not yet achieved orbital altitude. If the engine starting times (zero thrust to mainstage operati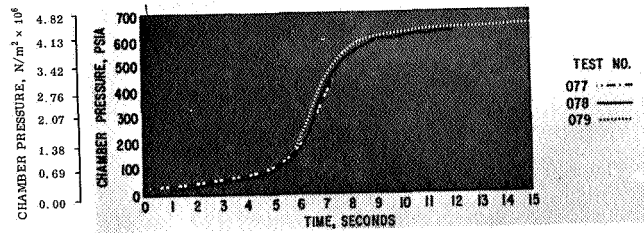on) are excessive, the payload capability will be de-graded. This would not appear to be critical for restart applications, typical of the S-IVB Stage, because orbital altitude has been achieved and extended operation in idle mode can be used as the mechanism for purging the warm propellants from the feed systems. This should not substract from the merits of developing tank head starting capability because the use of the SPTS for some missions (long duration between starts) could subject the solid propellant grains to environmental extremes and require thermal conditioning of the SPTS systems, thus rendering them impractical. In 1967, considerable effort will be concentrated on the tank head start capability because of the potential payoff.